

Thermoeconomic analysis of a novel topology of a 5th generation district energy network for a commercial user

Francesco Calise^a, Francesco Liberato Cappiello^{a,*}, Luca Cimmino^a, Maria Vicedomini^a, Fontina Petrakopoulou^b

^a DII - University of Naples Federico II, P.le Tecchio, 80 - 80125, Naples, ITALY

^b Department of Energy Engineering and Climate Protection, Technische Universität Berlin, Germany

HIGHLIGHTS

- Novel paradigm to be easily adopted by existing residential districts.
- The proposed novel paradigm is able to significantly reduce the primary energy consumption of the residential district.
- Very promising results with a primary energy saving index of 38% and payback period of 2.2 years.
- The power to heat strategy is able to further exploit the renewable electricity not directly exploited by the renewable energy community

ARTICLE INFO

Keywords:

District heating and cooling
5th generation district
Renewable energy systems
Photovoltaic panels
Dynamic simulation

ABSTRACT

This research compares an existing 4th generation heating and cooling network with a novel 5th generation heating and cooling network, driven by renewables. The networks are designed to cover the energy demand of a large shopping center. The existing network uses the thermal energy recovered from a trigenerative reciprocating engine coupled with an absorption chiller, to supply the heating and cooling networks. The proposed renewable 5th generation network consists of two neutral rings: the first one is the cold sink for the water-to-water heat pumps, installed in the substations; the second one is the hot sink for the heat pumps installed in the substations. One of the main novelties of the proposed layout consists in the use of a heat exchanger between these two rings. This heat exchanger recovers the heat rejected by the condensers of the heat pumps operating in cooling mode, supplying the evaporators of the heat pumps operating in heating mode. A photovoltaic field equipped with a lithium-ion battery partially matches the electricity demand of the network. The models of the shopping center and the existing and proposed networks are developed in TRNSYS environment. The proposed system achieves promising results: renewable electricity matches roughly 89% of the shopping mall electricity load can be covered by renewable power.

1. Introduction

District heating and cooling (DHC) technology is an increasingly appealing solution to reduce the primary energy consumption and CO₂ emissions in the residential sector [1]. District heating and cooling (DHC) networks underwent several innovations since they were first developed, and each renewal action marked the line between one generation and the following one [2]. In particular, every generation of DHC faced a significant decrease in its operating temperature, from 150 °C in the first generation [3] to about 55 °C – 65 °C of the 4th generation

district heating and cooling (4GDHC), down to a temperature close to the ambient temperature (between 15 °C and 25 °C) of the 5th generation district heating and cooling (5GDHC) networks [4]. Within this framework, the most significant innovations were introduced by the 4GDHC. In particular, the significant decrease of the operating temperature allows one to integrate into the network very efficient technologies, such as heat pumps (HPs). In addition, 4GDHC are specifically designed to be fed by both thermal (solar, geothermal, etc.) and electric (solar photovoltaic, wind) renewable energy sources. Moreover, they also represent a special case of polygeneration technologies, considered one of the most promising drivers for the transition toward fully

* Corresponding author.

E-mail address: francescoliberato.cappiello@unina.it (F.L. Cappiello).

| Nomenclature | |
|----------------------|------------------------------------------------------------------------------------------|
| A | area [m^2] |
| ACH | absorption chiller |
| AHU | air handling unit |
| C | operating costs [€/year] |
| CB | condensing boiler driven by natural gas |
| CH | electric chiller |
| CHP | cogeneration of heat and power |
| COP | coefficient of performance of split-system air conditioners [–] |
| c_p | specific heat at constant pressure [kJ/(kg K)] |
| C_{inv} | total capital cost [€] |
| DHC | district heating and cooling |
| E | energy [kWh] |
| F | CO_2 equivalent emission factor [kg CO_2 /kWh] |
| GHE | geothermal heat exchanger |
| GHG | greenhouse gases |
| H | heating |
| HE | heat exchanger |
| HP | heat pump |
| I | capital cost of the single component [€] |
| J,j | specific cost (purchasing) or price [€/kW or €/kWh or €/ Sm^3] |
| j_{CO_2} | specific carbon tax [€/kg $\text{CO}_{2,\text{eq}}$] |
| L | distance travelled by a single vehicle [m] |
| LIB | lithium-ion battery |
| LHV | Lower Heating Value [kWh/ Sm^3] |
| m | mass flow rate [kg s^{-1}] |
| m | percentage of the operating and maintenance cost with respect to the CAPEX cost [%/year] |
| M-HE | main heat exchanger |
| N_p | number of people [–] |
| NPV | Net Present Value [€] |
| NR | neutral ring |
| P | power [kW] |
| PE | primary energy [kWh/year] |
| PES | primary energy saving [–] |
| PI | profitability index [–] |
| PV | photovoltaic |
| Q | heat transfer rate [kW] |
| R | ratio |
| SPB | simple pay-back period [years] |
| T | temperature [°C] |
| U | overall heat transfer coefficient [W/(m ² K)] |
| WWHP | user cooling water loop |
| UWL | user water loop |
| V | volume [m^3] |
| WLHP | water loop heat pump |
| WWHP | water-water heat pump |
| <i>Greek Symbols</i> | |
| Δ | difference [–] |
| η | efficiency [–] |
| ρ | density [kg/m ³] |
| <i>Subscripts</i> | |
| aux | refers to auxiliary systems |
| B | refers to the boiler |
| C | compressor |
| CB | condensing boiler |
| cool | cooling |
| DHW | domestic hot water |
| LIB | district electric energy storage system based on lithium-ion technology |
| E | energy |
| el | electric |
| F | fraction |
| feed | feeding flow |
| fromLIB | refers to the electricity withdrawn from LIB |
| fromGRID | electric energy withdrawn from the public power grid |
| H | refers to building space heating demand |
| LOAD | electric demand |
| max | maximum |
| min | minimum |
| NG | natural gas |
| PS | proposed system |
| PV | photovoltaic |
| RS | reference system |
| SoC | state of charge |
| self | self-consumed electric energy |
| th | thermal |
| toLIB | refers to the electric energy delivered to D-LIB |
| toGRID | refers to the electric energy delivered to the public power grid |

decarbonized energy systems [5]. As 5GDHC rings operate at about the ambient temperature, they are also known as “neutral” rings [6] and the ground itself could represent a source of energy for these systems [7]. The concept of neutral ring arises from the possibility of operating with nearly ambient, and ground, temperatures to promote internal heat recovery in case of simultaneous heating and cooling demands.

5th generation district heating and cooling (5GDHC) are usually equipped with heat pumps (HPs) in the substations for meeting the user demands of the users. Such HPs can use the neutral ring as a hot, or a cold sink, significantly increasing the COP, with respect to conventional air-cooled HPs [8]. 5GDHC networks are extremely attractive for their capability to simultaneously supply heating and cooling energy using the same pipeline. Another crucial feature of 5GDHC systems is the bidirectionality of the energy flows, maximizing the energy recovery within the network, making the users also producers of energy, better known as “prosumers” [9]. Finally, 5GDHC systems have been receiving more attention due to the possibility to move to a fully electric district heating and cooling (DHC) system, by a massive utilization of HPs [10]. In particular, the development of HPs technology is a driver for the reduction of the operating temperature of DHC [11].

A number of different arrangements are available in literature for 5th generation district heating and cooling (5GDHC) systems, supplying space heating and cooling and domestic hot water (DHW), based on different technologies and operating temperatures of heat pumps (HPs). In many cases, booster HPs for DHW and low temperature rings for space heating and cooling is a promising solution [12]. Their high capital costs, the lack of clear guidelines, and the absence of business models are some drawbacks preventing the wider implementation of 5GDHCs [13]. Moreover, there is a general misconception about the differences between 4th generation district heating and cooling (4GDHC) and 5GDHC since both options can coexist to reach the decarbonization goals, being both featured by several pros and cons [14]. The number of works available in literature dealing with 5GDHC is significantly lower compared with the ones regarding 4GDHC, meaning that a significant research effort must be performed to promote the massive utilization of such technology. In the case of 4GDHC, the operating supply and return temperatures are significantly higher compared to the 5GDHC case, ranging between 55 °C – 60 °C and 25 °C – 30 °C, respectively [15]. In the past few years, both district heating and district cooling networks underwent a remarkable innovation process [15]. An important step in

the development of the technology was also due to the integration of renewable energy systems in the network [16,17], which dramatically increased the plant performance [18]. Several works are available in the open scientific literature, integrating renewables in energy networks [19], such as: HPs fed by photovoltaics [20] or wind turbines [21]. Moreover, in the framework of the Power-to-Heat (P2H) processes, several technologies are investigated, such as solar thermal collectors [22], geothermal heat pumps (GHPs) [23,24], anaerobic digesters and pyrogasifiers [25], low-temperature cogeneration of heat and power (CHP) [26], and industrial waste heat [27]. Unfortunately, 4GDHC systems are generally featured by centralized heat generation, being mostly an upgrading of 3rd generation district heating and cooling (3GDHC). This point can affect the system reliability [28]. This issue has been overcome with the 5GDHC technology [29].

1.1. District heating and cooling modelling and simulation

The simulation of district heating and cooling (DHC) networks is a challenging task because of the large number of components and devices included in such plants [30]. Some authors simulated the systems using commercial simulation platforms (TRNSYS, ENERGYPLUS, EnergyPLAN, etc.), showing very different features and capabilities [30]. Several authors found interesting solutions to provide fast-time dynamic simulation models [31–33]. In Sorknaes et al. [34], a comparison between 3rd generation district heating and cooling (3GDHC) and 4th generation district heating and cooling (4GDHC) networks is made by means of EnergyPLAN software. The simulation for the district of Aalborg, in Denmark, mainly regarded the analysis of the thermal losses and the integration of thermal storage. The 4GDHC solution was more profitable from both energy and economic points of view but it was characterized by a higher complexity and a more challenging design. The simulation of the 5th generation district heating and cooling (5GDHC) was particularly complex due to the bidirectional arrangement [35]. Generally, simplified modelling approaches are developed, as in Ref. [36], where a 5GDHC integrating Borehole Heat exchangers (BHE) for seasonal thermal storage was analyzed. The model calculated the levelized cost of energy, the capital cost, the greenhouse gases emissions, the exergy efficiency, and the electricity peak power of the system, for a case study including 305 buildings. BHEs have a positive impact on the mentioned factors but the relevant drilling costs still represent a severe issue. Novel modelling approaches of 5GDHCs aim to improve the calculation time and accuracy with respect to more conventional software, such as MODELICA [33].

A relevant work based on INTEMA, which is a tool developed in MODELICA [37], was proposed by Bellos et al. [38]. In this work, authors developed a suitable simulation model of both centralized and decentralized district heating and cooling (DHC) including thermal storage. A novel control strategy applied to decentralized thermal storage was proposed, with the scope to minimize the thermal losses and the energy demand of the grid. The validation of the model was performed, comparing the results with measurements of data for a real case study with centralized storage consisting of 9 dwellings located in Austria, equipped with underfloor heating systems. The authors concluded that the proposed decentralized layout achieves 18% energy savings and a reduction of thermal losses equal to 22%. Optimization tools are therefore crucial when developing the design of these technologies, as also shown in other works [39]. Dynamic models are useful to investigate the performance of DHC systems integrating renewables, like photovoltaic-thermal (PVT) [40], geothermal [41], and solar-geothermal [42]. The wider use of renewables in DHC systems also led to the development of more accurate models for thermal energy storage (TES) [43], to balance energy production and demand [44]. MODELICA was also used in Ref. [45] to show the effect of the heat distribution inside the building on the energy performance of a 5th generation district heating and cooling (5GDHC). The work concluded that the temperature of the fluid significantly impacts the overall network energy

demand, whereas the power consumption of circulating pumps is often negligible.

Dynamic simulations of 4th generation district heating and cooling (4GDHC) systems are mostly developed in TRNSYS environment. In a recent study by Testasecca et al. [46], the authors developed a detailed transient model for a thermal network with prosumers. The model was applied to a case study of a system serving 10 users (schools, offices, apartments, hotels, hospitals, etc.) with dual heating and cooling loops powered by a trigeneration system and an absorption chiller. The model simulates real-time operations and measures the energy flows and pressure losses. The considered scenarios include 3rd generation district heating (3GDH) at 100 °C, 80 °C, and 60 °C, and 4th generation district heating (4GDH) (between 60 °C and 70 °C) with prosumers and solar thermal collectors. Results show that thermal losses significantly affect the plant energy balance. When the 3GDH temperature decreases from 100 °C to 80 °C, the losses are reduced by 27%, and when the temperature decreases from 100 °C to 60 °C, the losses are reduced by 53%. TRNSYS was also used by Bordignon et al. [40] to develop a novel ultra-low temperature district heating and cooling (DHC) layout. The system is based on the use of a ground source heat pump for the main loop of the DHC system and dedicated substations including water-to-water heat pumps (WWHPs) and PVT collectors for each building. Results of simulations carried out under different weather conditions showed that in cold weather conditions, photovoltaic-thermal (PVT) collectors can supply only a small amount of the overall thermal energy demand (e.g. 16% in Helsinki). Conversely, this share increases up to 25% in the warmer weather conditions (Strasbourg).

A combination of TRNSYS and Fluidit Heat was used by Saini et al. [47] to perform a techno-economic analysis of a 5th generation district heating and cooling (5GDHC) located in Tallinn. A Monte Carlo optimization algorithm was implemented in Python to analyze the sensitivity of the economic performance of the system. The network was based on a loop operating at 20–25 °C, supplied by waste heat provided by industries. Each building was equipped with a substation, including heat pumps (HPs) for space heating and cooling and for domestic hot water (DHW). The system is featured by a total heating load of 2.43 GWh/year with a heat pump seasonal COP of 3.3, consuming 0.76 GWh/year of electricity. They estimated a capital expenditure of 1.7 M€, with operating costs for heating of 80 €/MWh. The most likely heating cost is 85.4 €/MWh, spanning from 58.8 to 117 €/MWh, with a 74.5% chance of price increases due to input variability.

In a previous work [48] by the same authors, a dynamic simulation of a 5th generation district heating and cooling (5GDHC) developed in TRNSYS environment is proposed. The system included two low-temperature bidirectional rings balanced by means of seawater heat pumps (HPs). The calculations showed important energy savings, but a poor economic profitability with payback times longer than 15 years. In Calise et al. [48], a 5GDHC model was developed in TRNSYS environment for the residential district of Leganés (Madrid, Spain). In this case, a residential user was considered with an accurate characterization of the time-dependent heating, cooling, and DHW demands. Here, the neutral rings were balanced by means of geothermal heat exchangers (GHE) and water-to-water heat pumps (WWHP). A photovoltaic (PV) field was used to partially meet the energy demand of the user. The primary energy saving (PES) of the system and the savings in CO₂ emissions were 64% and 76%, respectively. The PV matched 30% of the total electricity demand. In this case, the economic feasibility was even poorer, as the relevant drilling and installation costs of the geothermal heat exchangers, leading to a Simple Payback (SPB) of 33 years. In a more recent work [49], authors also developed a 4th generation district heating (4GDH) layout and compared it to the 5GDHC layout proposed in [48]. In both cases the systems were equipped with a PV field and Lithium-Ion batteries to partially meet the electricity demand of the user. The comparative thermoeconomic analysis of the districts showed that the 4GDHC had a better performance compared with the 5GDHC. The authors proved that this result mainly relies on the peculiarities of

the selected user served by the district heating and cooling (DHC). In this case, a residential district was considered. The residential district is featured by an extremely limited simultaneous heating and cooling demands. Therefore, no relevant advantage was achieved by the use of the neutral ring. Furthermore, the additional capital cost of the heat pumps was not suitably balanced by the lower operating costs.

1.2. Aim and novelty of the paper

The analysis of the scientific literature proposed above shows that in the open literature there is a lack of guidelines for properly developing 5th generation district heating and cooling (5GDHC) [10]. In addition, only a few works analyze the dynamic performance of the integration of renewable 5GDHC with non-residential users. In this framework, this paper proposes a novel 5GDHC layout to meet the thermal energy demand of a large shopping mall located in Madrid.

The 5th generation district heating and cooling (5GDHC) proposed in this research consists of two neutral rings: neutral ring 1 (NR1) acting as the cold sink for the heat pumps operating in heating mode, and neutral ring 2 (NR2) operating as the hot sink for the heat pumps operating in cooling mode. The heat exchange between the two rings is allowed by means of the main heat exchanger. A similar layout was proposed in a previous work [49]. However, compared to the previous research, the new layout proposed in this work shows several significant improvements. First, the novel layout proposed here includes a completely new component arrangement that improves the heat exchange between the two neutral rings. In particular, the water stream leaving the evaporators of the water loop heat pumps operating in heating mode is directly supplied to the main heat exchanger. This stream exchanges directly with the water stream leaving the condensers of the heat pumps operating in cooling mode. In this way, the heat transfer between the two rings is maximized. Moreover, this heat exchange is also beneficial for the operating source temperature of both heat pumps operating in heating and cooling modes. The second novel point concerns NR2, which is balanced by means of a group of cooling towers vs a dedicated air-to-water heat pump (AWHP). This measure is designed to further reduce the electricity consumption of the district heating and cooling (DHC). The main novelties of the work are summarized below.

- A completely novel topology of a 5GDHC based on two neutral rings.
 - The warm neutral ring is balanced with cooling towers, the performance of which is carefully analyzed to also evaluate the consumption of demineralized water.
 - The energy features and performance of the shopping mall are carefully and dynamically modelled.
 - Dynamic analysis of the 5GDHC integrated with a non-residential user, lithium-ion battery, and photovoltaic field.
 - Thermo-economic analysis of the proposed system to assess the economic and environmental benefits of the proposed novel layout.

2. System layout

Fig. 1 shows the existing layout, developed for matching the electric and thermal energy demands of the user, i.e., a large shopping mall located near Madrid. The shopping mall includes several facilities that need both heating and cooling energy. Especially during the winter months there is a simultaneous demand for space cooling energy and space heating energy from different zones of the building. This point is addressed in detail in the section *Case Study*.

This layout consists of a conventional power plant based on an internal combustion engine cogenerator (CHP) of 1.50 MW, simultaneously supplying thermal and electric energy. The electricity produced by the engine is used for matching a fraction of the power load of the user. Note that this plant also includes a small PV field. The thermal energy recovered from the CHP matches the user thermal energy demand. In particular, the water flowing into the jacket of the engine, i.e. jacket water, delivers the heat to the heating water, which drives the main heat exchanger. Thus, the recovered thermal energy is supplied to the user water loop (UWL) by means of the main heat exchanger (M-HE). The heating and cooling load is met by several air handling units (AHUs).

The user water loop (UWL) directly feeds the air handling units (AHUs) operating in heating mode. In particular, this hot water stream, i.e. UWL, is delivered to the AHUs coils heating the air passing into the AHUs. Conversely, when the AHUs are in cooling mode, the UWL supplies hot water to an absorption chiller (ACH) which produces chilled water (CW). This chilled water is supplied to the AHUs. Note that several

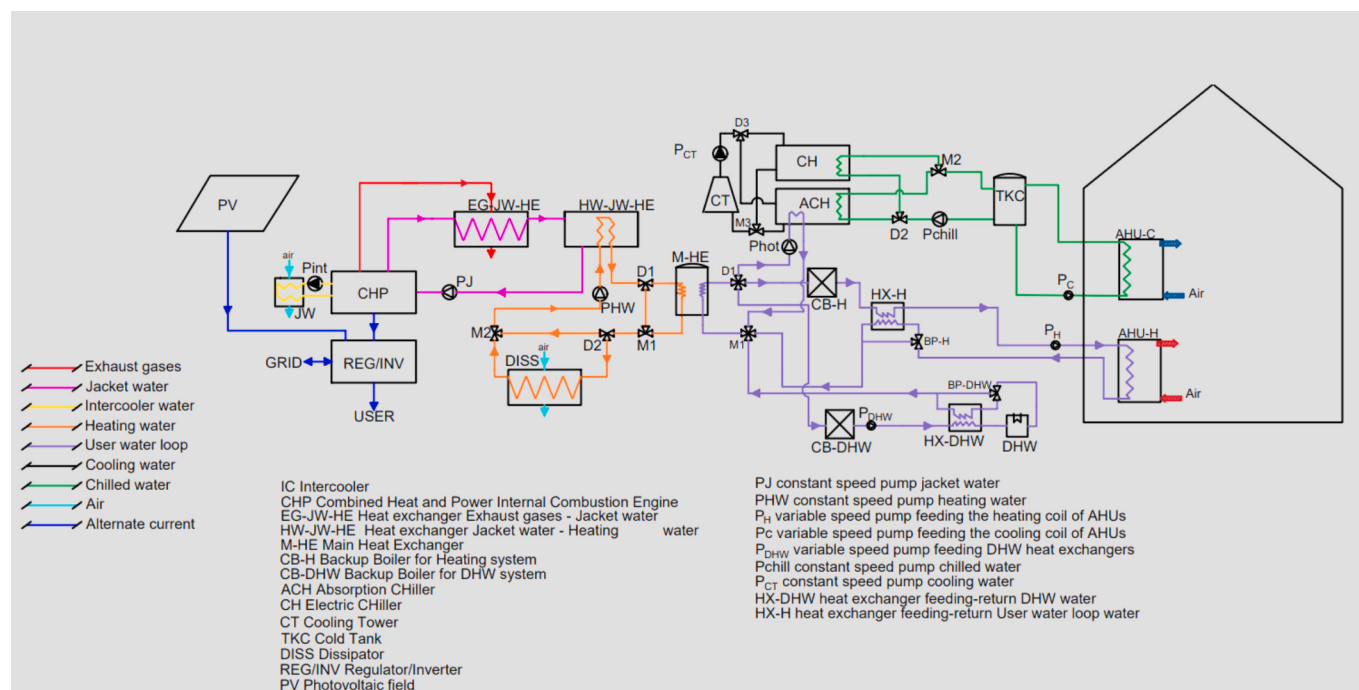


Fig. 1. Existing layout

thermal zones are considered. Therefore, some AHUs may operate in heating mode and other AHUs may operate in cooling mode. The plant is able to simultaneously supply the AHUs operating in heating and cooling modes. A natural gas fired boiler (CB-H) is also included as an auxiliary system. This CB-H is designed to achieve a minimum AHUs supply temperature of 42 °C during the heating mode operation. Note that a heat exchanger is installed between the supply water branch and return water branch. When the UWL supplying water temperature is above the set point, a proportional controller turns on the diverter BP-H, delivering part of the water mass flow rate to the heat exchanger HX-H. This control strategy keeps the temperature of the UWL below the maximum set point of 50.0 °C, without wasting thermal energy. The design temperature of the AHU supplying air is assumed to be equal to 35.0 °C. The water mass flow rate of UWL delivered to the AHUs coils is managed by feedback controllers, which select the suitable amount of water supplied to the AHUs coils to steer the temperature of the outlet air of the AHU to 35.0 °C.

An electric chiller (CH) is also included in the existing plant as an auxiliary system for the air handling units (AHUs) when the cooling energy provided by the absorption chiller (ACH) is limited or null. In fact, the thermal energy recovered from the cogenerator (CHP) is firstly used for heating purposes, meaning that it may not always be sufficient for driving the absorption chiller (ACH) at its rated capacity. The chilled water loop is designed for operating within the rated temperature range of 10.0 °C – 15.0 °C. The set point temperature of the AHUs supply air is assumed to be equal to 18.0 °C. The chilled water mass flow rate delivered to the coils of the AHUs operating in cooling mode is selected by feedback controllers. These controllers are designed to meet the AHUs cooling energy demand with the minimum water mass flow rate.

The thermal energy produced by the cogenerator (CHP) is also used to meet the domestic hot water demand. The user water loop (UWL) heats the required amount of domestic hot water (DHW) by means of a water-to-water heat exchanger. A boiler is also considered as an auxiliary system (CB-DHW).

Fig. 2 displays the proposed layout, i.e., a 5th generation district heating and cooling (5GDHC) network driven by air-to-water heat pumps (AWHPs), cooling towers, water-to-water heat pumps and a photovoltaic field. This 5GDHC network includes two neutral rings: neutral ring 1 (NR1) and neutral ring 2 (NR2). NR1 represents the cold sink of the heat pumps operating in heating mode, and it is featured by a temperature ranging between 15.5 °C and 18.0 °C. This ring provides

thermal energy to the evaporators of the heat pumps operating in heating mode. NR2 represents the hot sink of the heat pumps (HPs) operating in cooling mode. Then, the condensers of the heat pumps operating in cooling mode supply thermal energy to this ring. This ring is designed with a rated range of temperatures equal to 18.5–24.0 °C.

Neutral ring 1 (NR1) is balanced by means of an air-to-water heat pump (AWHP) of 6.29 MW_{th}. In particular, a suitable control strategy manages the operation of NR1. When the temperature of the ring NR1 (T_{NR1}) decreases below the minimum allowed value of 15.5 °C, the heat pump M-HP1 is activated, until T_{NR1} approaches the maximum allowed temperature of 19.0 °C.

Neutral ring 2 (NR2) is balanced by means of a group of three cooling towers of 3.60 MW. These cooling towers are designed to keep the temperature of the ring within the rated range of 18.5–24.0 °C. Therefore, when the temperature of the ring NR2 (T_{NR2}) rises above the maximum allowed value of 24.0 °C, the cooling towers are activated until the temperature of the NR2 reaches the value of 18.5 °C. During the summer period, when the thermal energy discharged from the condensers of the water loop heat pumps operating in cooling mode (WLHPs-C) is very high, the temperature of NR2 could rise above the rated value of 24.0 °C. In fact, the cooling towers are not able to steer the temperature of NR2 within the rated range, due to the high ambient temperature and humidity. However, this issue does not significantly affect the operation of the plant. In fact, the WLHPs-C are designed for operating with a condenser source temperature ranging between 10.0 °C and 45.0 °C. Obviously, this leads to a reduction of the COP of WLHPs-C. The demineralized water consumption of the cooling towers is also considered. The system includes a reverse osmosis (RO) module that produces demineralized water supplied to the cooling towers to replace the evaporated water.

Neutral ring 1 (NR1) provides thermal energy to the evaporators of the water loop heat pumps operating in heating mode (WLHPs-H). In particular, WLHPs-H heat up the user heating water loop (UHWL), which is delivered to the coils of the AHUs. An on-off controller manages each WLHP-H. When the temperature of user heating water loop (T_{UHWL}) drops below 42.0 °C, the WLHPs-H are activated until T_{UHWL} reaches the value of 50.0 °C. Therefore, the pump P5 is activated to deliver the NR1 water to the WLHPs-H evaporator, and the P9—H is activated to deliver the water heated by WLHPs-H to UHWL.

The air handling units (AHUs) operating in cooling mode are fed by the User Cooling Water Loop (UCWL), designed to range from 10.0 °C to

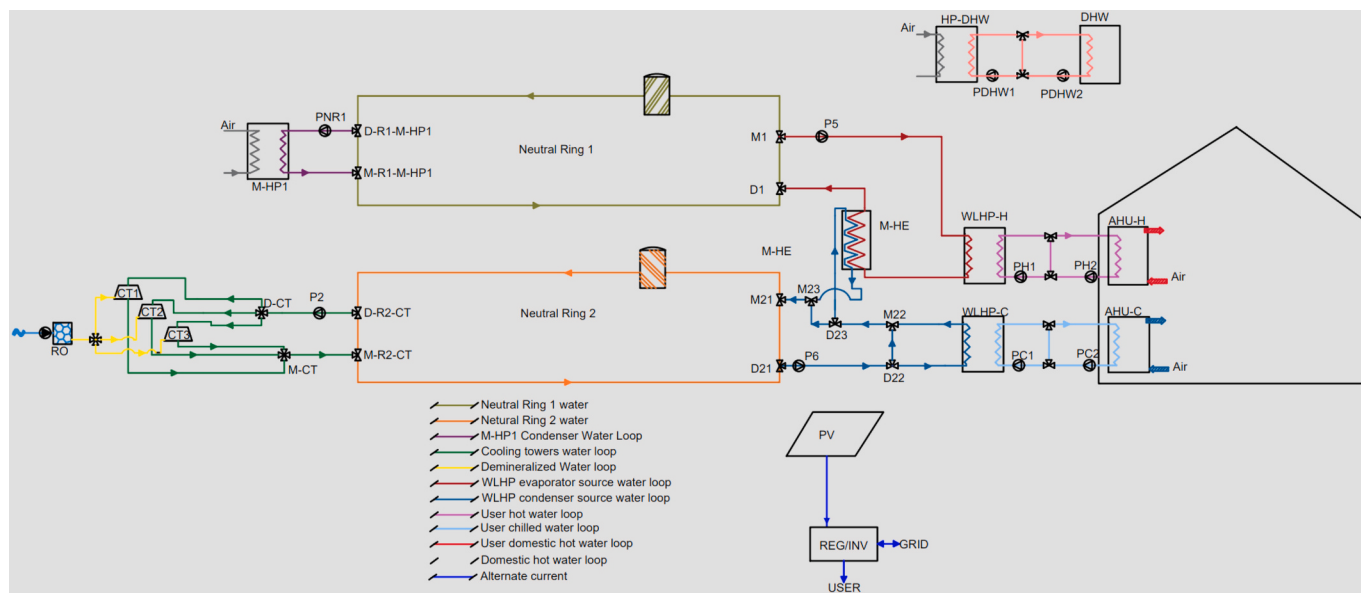


Fig. 2. Proposed layout.

15.0 °C. Therefore, when the temperature of the user cooling water loop (T_{UCWL}) rises above 15.0 °C, the water loop heat pumps operating in cooling mode (WLHPs-C) are activated to decrease T_{UCWL} down to 10.0 °C. At the same time pump P6 is activated, supplying the water of NR2 to the condensers of the water loop heat pumps operating in heating mode (WLHPs-H), which supplies heat to this water stream.

The main heat exchanger M-HE is designed to allow the heat transfer from neutral ring 2 (NR2) to neutral ring 1 (NR1). This heat exchange is the conceptual core of the proposed 5th generation district heating and cooling (5GDHC) network. In particular, this heat exchange increases the temperature of NR1, limiting the activation of M-HP1. The increase of NR1 temperature also enhances water loop heat pumps operating in heating mode (WLHPs-H) performances. Here, the evaporators of the heat pumps are fed by the NR1 water: the higher the temperature of the water delivered to the evaporators, the higher the COP. At the same time, this heat exchange allows NR2 to discharge the heat supplied by the condenser of the water loop heat pumps operating in cooling mode (WLHPs-C), limiting the activation of the cooling towers CTWs. In addition, the lower the NR2 temperature, the better the WLHPs-C performance is. In fact, when the temperature of the water supplied to the condenser of the heat pumps operating in cooling mode decreases, the performance of the heat pumps increases. The control strategies managing this heat exchange are discussed in the section *System Model*.

The domestic hot water (DHW) demand of the shopping mall is met by a separated 4th generation district heating and cooling (4GDHC) network. Given the much lower thermal energy demand for DHW compared to the other thermal energy demands, this ring is not included in the 5th generation district heating and cooling (5GDHC) network serving the mall. The DHW loop is balanced by a dedicated air-to-water heat pump (HP-DHW).

The layout also includes a photovoltaic (PV) field equipped with a lithium-ion battery (LIB) in order to increase the share of energy self-consumed. The tanks reported in Fig. 1 and Fig. 2 represent the inertia of the piping network serving the mall.

The temperatures of each loop, here reported, are the design temperatures of each loop, therefore those are input data for the model. These values can be modified by the system manager and be subjected to any optimization, as a function of the boundary conditions (weather, energy costs, loads, etc.). Such temperatures are used to set the controllers designed to steer the temperatures of the loops within the design ranges discussed.

3. System model

The dynamic simulation models of both the existing and proposed power plants serving the shopping mall are developed in TRNSYS 18. TRNSYS is widely adopted in academic and commercial applications, as it is considered highly reliable and accurate for modelling and simulating complex energy systems based on renewables [46,48,50–54]. The validation of the developed systems as a whole is not possible, since the proposed system has not been installed yet, due to the large capacity and high capital costs. However, the simulation model includes a number of components (pumps, heat pumps, building, etc.) that are individually validated against experimental data and/or literature data. Most of these models are derived from validated libraries available in TRNSYS. Therefore, even if the validation of the overall system is not possible, the validation of each of the components included in the systems allows one to consider the model of the system, as a whole, intrinsically validated. This approach has been adopted in a large number of studies and is considered reliable and accurate [54–57].

The geometric model of the selected shopping mall was developed in Google Sketchup and TRNSYS3D. The geometric parameters are defined by means of on-site inspections. The geometric model is imported into the TRNSYS 18 environment by means of type 56 to simulate the energy performance of the building. The building type is integrated with several libraries in order to model the complete existing and proposed plants.

Table 1
Main libraries adopted in the work.

| Library | Model |
|----------|---------------------------------------|
| Type 56 | Building model |
| Type 941 | Single-stage air-to-water heat pump |
| Type 927 | Single stage water-to-water heat pump |
| Type 3 | Fixed speed pump |
| Type 80 | Diverter |
| Type 76 | Mixer |
| Type 5 | Cross flow heat exchanger |
| Type 75 | Piping network |
| Type 51 | Cooling tower |
| Type 647 | Feeding Manifold |
| Type 649 | Return Manifold |

Table 1 summarizes the main libraries included in the developed models. For the sake of brevity, only a brief description of the main components is provided.

- Type 56 allows the user to evaluate the thermal load and simulate the dynamic energy performance of the building. It is also possible to divide the building into different thermal zones. This type considers the indoor heat gain, the solar gain, the envelope thermophysical properties, the orientation of the building, and the 3-D geometry. For a detailed description see Ref. [58].

- Type 941 models a single-stage air-to-water heat pump (AWHP). The HP can work both in heating and cooling mode, heating up (cooling down) a water stream by withdrawing energy from (rejecting energy to) the air stream. This type provides the power consumption and the heating or cooling capacity based on user-supplied data files containing catalogue data. A detailed description is provided in Ref. [59].

- Type 927 models a single stage water-to-water heat pump. This type defines normalized heating or cooling capacity and the power load based on user-supplied data files. Type 927 receives as input the entering load and source temperature and the normalized source and load flowrates returning the heating/cooling capacity, the power demand, and the temperatures of the outlet streams. For further details see Ref. [48].

3.1. Main heat exchanger control strategy

The main heat exchanger (M-HE), Fig. 2, allows the heat transfer from the neutral ring 2 (NR2) to the neutral ring 1 (NR1). More specifically, the condensers of the water loop heat pumps operating in cooling mode (WLHPs-C) supply heat to the evaporators of the water loop heat pumps operating in heating mode (WLHPs-H). Fig. 3 presents the control strategy for the M-HE. In particular, when the WLHPs-H are in operation, the water flow rate exiting the WLHPs-H evaporators ($m_{NR1,return}$) is delivered to the main heat exchanger (M-HE in Fig. 2). At the same time, if the WLHPs-C are in operation and the temperature of the water exiting the condensers of the WLHPs ($T_{NR2,return}$) is greater than the temperature of the water mass flow rate exiting the evaporators of the WLHPs-H ($T_{NR1,return}$), the diverter D23 (Fig. 2) is activated, allowing the water flow rate exiting the WLHPs-C condensers to flow into the M-HE. In this way, NR2 discharges heat to NR1.

However, if the water loop heat pumps operating in heating mode (WLHPs-H) are in operation but the water loop heat pumps operating in cooling mode (WLHPs-C) are not in operation, the heat exchange is performed directly with the water withdrawn from the neutral ring 2 (NR2). Therefore, the pump P6 is activated, and the diverter D22 directly diverts the NR2 water to the main heat exchanger, bypassing the water loop heat pumps operating in cooling mode (WLHPs-C) condensers (see also Fig. 2).

Note that this heat exchange is only allowed while $T_{NR2,return}$ is greater than $T_{NR1,return}$.

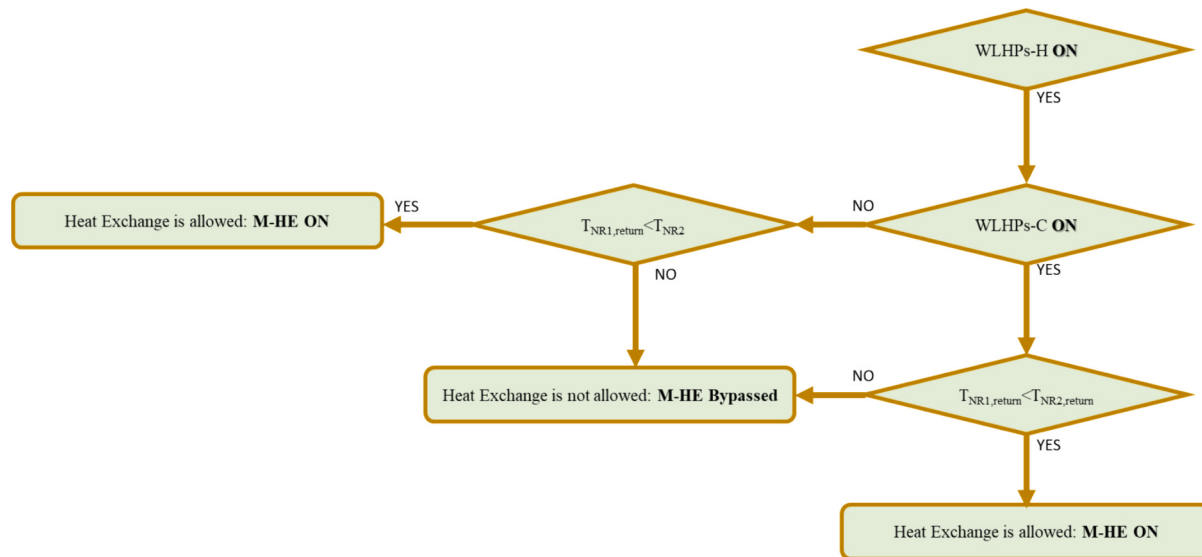


Fig. 3. Control strategy regarding the main heat exchanger M-HE: $T_{NR1,return}$ is the return temperature of NR1, $T_{NR2,return}$ is the return temperature of NR1, T_{NR2} is the temperature of NR2.

Table 2
Design and operating parameters.

| Parameter | Description | Value | Unit |
|-------------------|----------------------------------------------------------------------|---------------------------------------------------|---------------------------|
| J_{PV} | PV specific cost | 1.00 [49] | k€/kW |
| J_{HP}/J_{WLHP} | Heat pump and water loop heat pump specific cost | 0.15 [48] | k€/kW |
| J_{piping} | Specific piping cost | 90 [60] | k€/km |
| C_{pumps} | Cost of hydronics pumps | 272 [61] | k€ |
| J_{M-HE} | Specific cost of M-HE | $C_{HE} = 182 \cdot [(A_{HE}/0.093)^{0.78}]$ [62] | k€ |
| J_{LIB} | Specific lithium-ion battery cost | 200 [49,63] | k€/MWh |
| η_{el} | Conventional thermo-electric power plant efficiency | 0.498 [48] | – |
| η_{CB} | Boiler efficiency | 0.86 | – |
| $J_{el,fromGRID}$ | Electricity purchasing cost | 0.09 [64] | €/kWh |
| $J_{el,toGRID}$ | Electricity selling price | 0.02 [64] | €/kWh |
| J_{NG} | Natural gas purchasing cost | 0.53 [65] | €/Sm ³ |
| j_{water} | Water purchasing cost | 1.00 | €/m ³ |
| m_{CHP} | Cogeneration maintenance cost | 1.00 [50] | %/year |
| m_{PV} | Photovoltaic maintenance cost | 1.00 [49] | %/year |
| m_{DHC} | District heating cooling network maintenance cost | 1.00 | %/year |
| F_{el} | Equivalent CO ₂ emissions coefficient for natural gas | 0.200 [66] | kgCO _{2,eq} /kWh |
| F_{NG} | Equivalent CO ₂ emissions coefficient for electric energy | 0.190 [48] | kgCO _{2,eq} /kWh |
| AF | Annuity Factor | 14.09 | years/€ |

3.2. Thermo-economic model

The primary energy of the existing (reference) plant is described with the following equations.

$$PE_{RS} = \frac{E_{el,fromGRID} - E_{el,toGRID}}{\eta_{el}} + (V_{NG,CHP} + V_{NG,Aux}) \cdot LHV_{NG} \quad (1)$$

$$V_{NG,Aux} = \left(\frac{E_{th,CB-H}}{\eta_{CB-H}} + \frac{E_{th,CB-DHW}}{\eta_{CB-DHW}} \right) \left(\frac{1}{LHV_{NG}} \right)$$

where $V_{NG,CHP}$ and $V_{NG,Aux}$ are the natural gas consumptions by the cogenerator and by the auxiliary boilers, respectively (see Fig. 1). $E_{th,CB-H}$ and $E_{th,CB-DHW}$ are the thermal energy provided by the boilers CB-H and CB-DHW, respectively. η_{CB-H} and η_{CB-DHW} are the efficiency of the CB-H and the CB-DHW, respectively. η_{el} is the conventional thermo-electric power plant efficiency in Italy (.

Table 2). LHV_{NG} is the lower heating value of natural gas. $E_{el,fromGRID}$ and $E_{el,toGRID}$ are the electricity withdrawn from and supplied to the grid,

respectively. The main terms of these equations are presented in.

The primary energy of the proposed system is described with the following equations.

$$PE_{PS} = \frac{E_{el,fromGRID} - E_{el,toGRID}}{\eta_{el}} \quad (2a)$$

$$R_{fossil} = \frac{E_{el,fromGRID} E_{el,toGRID} \eta_{el}}{R_{fossil}} \quad (2b)$$

$$PES = \frac{PE_{RS} - PE_{PS}}{PE_{RS}} \quad (2c)$$

Note that the proposed system is based on electricity, therefore the volume of natural gas is zero (see Fig. 2). R_{fossil} represents the share of user primary energy demand balanced by means of renewable energy, whereas R_{fossil} is the share of non-renewable energy used to match the mall primary energy demand. PE_{RS} and PE_{PS} are the terms of primary energy consumed in the reference system and proposed system,

respectively.

The environmental impact of the reference and proposed systems in terms of avoided equivalent CO₂ emissions are assessed as follows.

$$\begin{aligned} CO_{2,RS} &= \left(\frac{E_t h, CB - H}{\eta_{CB-H}} + \frac{E_t h, CB - DHW}{\eta_{CB-DHW}} \right) F_{NG} + (E_e l, fromGRID - E_{el,toGRID}) F_{el} \\ CO_{2,PS} &= (E_e l, fromGRID - E_{el,toGRID}) F_{el} \\ \Delta CO_2 &= \frac{CO_{2,RS} - CO_{2,PS}}{CO_{2,RS}} \end{aligned} \quad (2d)$$

The equivalent CO₂ emissions factors for electricity withdrawn from the grid and natural gas consumption, F_{el} and F_{NG} , respectively, are shown in.

The operating costs of the reference system (RS) and the proposed system (PS) are evaluated as follows.

$$\begin{aligned} C_{RS} &= E_{el,fromGRID} j_{el,fromGRID} - E_{el,toGRID} j_{el,toGRID} + (V_{NG,CHP} + V_{NG,Aux}) j_{NG} + m_{CHP} + m_{DHC} + m_{PV} \\ C_{PS} &= E_{el,fromGRID} j_{el,fromGRID} - E_{el,toGRID} j_{el,toGRID} + m_{DHC} + m_{PV} + j_{water} M_{water} \end{aligned} \quad (3)$$

where $j_{el,fromGRID}$ and j_{NG} are the purchasing cost of electricity and natural gas, respectively, m_{CHP} is the maintenance cost of the cogenerator, m_{DHC} is the maintenance cost of the district heating network, including the maintenance cost of heat pumps, hydronic pumps, etc. (.

Table 2), m_{PV} is the maintenance cost of the photovoltaic field. As explained in the section *System Layout*, this models also includes the water consumption due to the cooling towers: j_{water} represents the specific water purchasing cost and M_{water} the water demand of the cooling towers.

The capital cost of the proposed system (C_{inv}) is assessed with the following equation.

$$C_{inv} = I_{PV} + I_{HPS} + I_{TK} + I_{pumps} + I_{LIB} + I_{piping} + I_{M-HE} \quad (4a)$$

The terms included in the equation are, in order, the capital costs for the photovoltaic field (PV), the heat pumps (HPS), the tanks (TK), the electric pumps (pumps), the lithium-ion battery (LIB), the piping (piping), and the main heat-exchanger (M-HE). All the main terms of the equations discussed are presented in.

Table 2. The considered lifespan of the system is 25 years, also considering yearly maintenance costs for the system. The same lifespan is assumed for all the main components included in the system. Therefore, no replacement costs are considered. A discount rate of 5% is also assumed, resulting in an annuity factor of 14.09 years (Table 2).

The simple payback is assessed as follows.

$$SPB = \frac{C_{inv}}{C_{RS} - C_{PS}} \quad (4b)$$

where C_{RS} and C_{PS} are the operating costs for the reference and proposed systems, respectively.

Sensitivity Analysis.

A sensitivity analysis is performed in order to assess how the PV field capacity and the battery capacity affect the performance of the proposed 5th generation district heating and cooling (5GDHC) based plant. Φ_{PE} is the primary energy objective function. According to Eq.(2a) this function can be negative, when the electricity exported is greater than the electricity withdrawn from the grid.

$$\Phi_{PE} = \frac{PE_{PS}}{PE_{RS}} \quad (5a)$$

Φ_{CO2} is the equivalent CO₂ emissions objective function of the proposed plant, also this term can be negative, see also Eq.(2c).

$$\Phi_{CO2} = \frac{CO_{2,PS}}{CO_{2,RS}} \quad (5b)$$

SPB is the economic performance objective function, see Eq.(4b).

In order to assess the performance of the system without considering the excess electricity exported to the grid, highlighting the contribution of the self-consumed energy, also R_{renew} and R_{fossil} are considered as object functions, see Eq.(2b).

In this paper, the optimization was performed using a simplified technique, successfully used by the authors in previous works [67]. This technique is based on computer-based Design of Experiments [68,69]. According to this approach, the decision variables assume discrete values ("levels", as shown in Table 3) and the simulations are performed for all the possible combinations (361) of levels of the two decision variables: namely the capacity of the battery and the capacity of the photovoltaic (PV) field (Table 3). Therefore, this technique allows one to calculate the shapes of the optimal response surfaces of all the considered objective functions with a very limited number of simulations. In fact, the optimization is performed using 361 simulations to achieve the

Table 3
Levels of the decision variables.

| Battery Capacity [MWh] | Photovoltaic field capacity [MW] |
|---------------------------|-------------------------------------|
| 2.70 | 5.40 |
| 3.24 | 6.47 |
| 4.32 | 8.63 |
| 5.40 | 10.80 |
| 6.48 | 12.96 |
| 7.56 | 15.12 |
| 8.64 | 17.29 |
| 9.72 | 19.43 |
| 10.80 | 21.59 |
| 11.88 | 23.76 |
| 12.96 | 25.92 |
| 14.04 | 28.08 |
| 16.20 | 30.25 |
| 17.28 | 32.39 |
| 18.36 | 34.55 |
| 19.44 | 36.72 |
| 20.52 | 38.88 |
| 21.60 | 41.04 |
| | 43.21 |

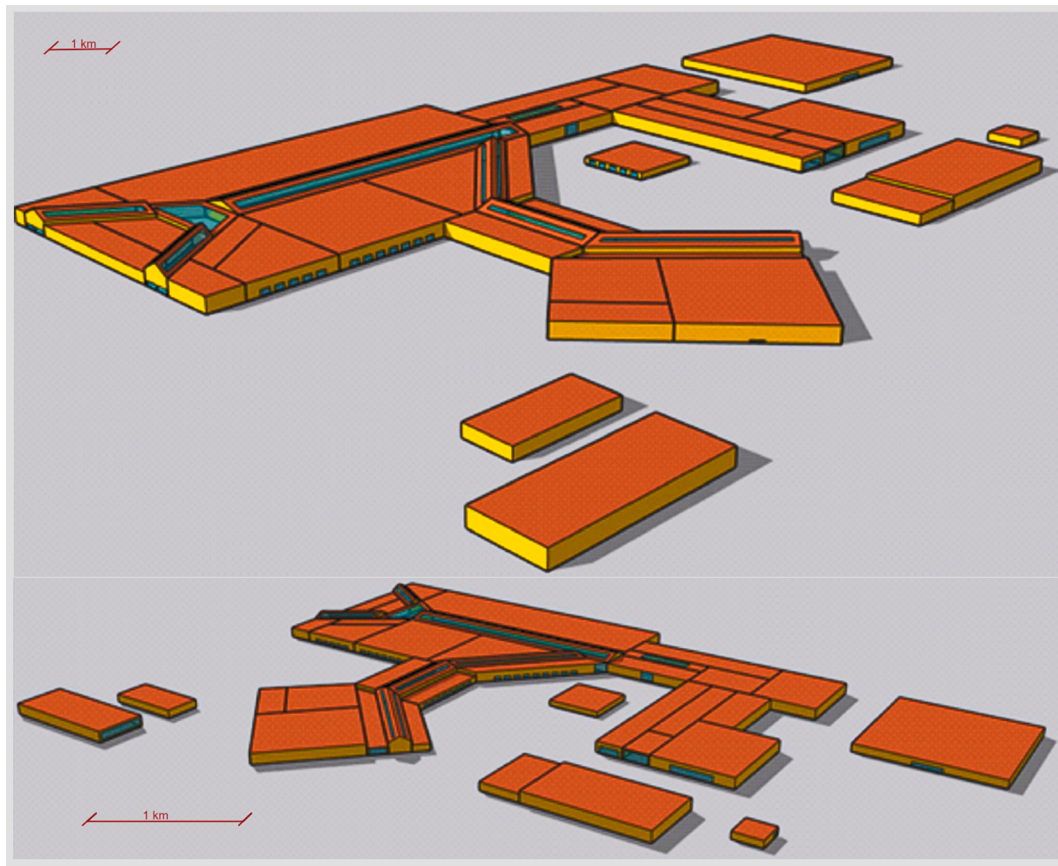


Fig. 4. 3D geometry of the shopping mall analyzed.

optimal configurations (using different objective functions) vs the 500–1000 simulations usually required to complete a conventional optimization for a single objective function. This technique showed a very good accuracy in engineering problems where the shape of the optimum response is not extremely discontinuous. In this specific case, the adopted technique allows one to reduce by a factor 4 the computational effort with respect to the built-in optimization tool (Genopt [70], developed by LBNL) included in TRNSYS package. Then, the multi-criteria optimization was completed implementing the well-known Pareto frontier analysis [71,72] which returns the optimal configurations, considering different conflicting objective functions. Note that the results of the TRNSYS simulations are used as input data for a script, developed in MATLAB, assessing the Pereto Frontier of the considered analysis. A detailed discussion regarding the Pareto frontier analysis is available in Refs. [71, 72].

In this framework, the tool TRNEDIT, included into the TRNSYS suite, is used for managing all the simulations to be performed. In particular, all the possible combinations of the levels, shown in Table 3, require 361 simulations: here, the input parameters of each simulation

Table 5

Heat gain parameters for the thermal zones defined in the shopping mall [15,76].

| Zone | Type | Heat Gain [W/m ²] | | | |
|----------------------|-----------|----------------------------------|----------------------------------|-------------------|------------------|
| | | | Power [W/ m ²] | Convective [%] | Radiative [%] |
| Gym | Equipment | 4.00 | 10.00 | 20.00 | 80.00 |
| Bowling | Equipment | 10.00 | 25.00 | 80.00 | 20.00 |
| Groceries | Equipment | 10.00 | 25.00 | 80.00 | 20.00 |
| Hallways | Equipment | 13.00 | 32.50 | 80.00 | 20.00 |
| Stores | Equipment | 10.00 | 25.00 | 80.00 | 20.00 |
| Clothing stores | Light | 11.30 | 22.60 | 79.99 | 20.01 |
| Jewelry Stores | Light | 20.20 | 40.40 | 80.01 | 19.99 |
| Electronics shops | Light | 5.00 | 10.00 | 80.00 | 20.00 |
| Bowling | Light | 10.00 | 20.00 | 80.00 | 20.00 |
| Cinema | Light | 2.90 | 5.80 | 79.98 | 20.02 |
| Gym | Light | 8.18 | 16.36 | 80.00 | 20.00 |
| Restaurant | Light | 9.25 | 18.50 | 80.00 | 20.00 |
| Hallway | Light | 10.00 | 20.00 | 80.00 | 20.00 |

Table 4
Characteristic features of the shopping mall envelope.

| Building element | Building | | | |
|------------------|------------------------------|-------------------|-----------------|-------------------|
| | U-value [W/m ² K] | Thickness [m] | ρ_s [-] | ϵ [-] |
| Facades | 0.620 | 0.380 | | |
| Adjacent ceiling | 1.665 | 0.190 | | |
| Floor | 0.658 | 0.375 | 0.400 | 0.900 |
| Roof | 0.380 | 0.330 | | |
| Windows glass | 2.72 | 0.006/0.016/0.004 | 0.472 | 0.190 |

are the combinations of decision variables, i.e. the capacity of the PV field and the capacity of the battery. Note that each simulation takes about 15 min, with a PC including a processor i7–7700 @ 3.60 GHz and a RAM of 8 GB. The simulation time may change due to the input parameters.

4. Case study

The selected user is a large shopping mall located in Leganés, Madrid, Spain. This mall consists of several shops of various types:

Table 6

Heat gains related to the consumers of the shopping mall [16,76].

| | Heat Gain [W/m ²] | Convective [%] | Radiative [%] | Latent [kg/h] |
|-----------------------|----------------------------------|-------------------|------------------|------------------|
| Clothes Store Users | 15.12 | 42.00 | 58.00 | 0.10 |
| Groceries Users | 29.16 | 42.00 | 58.00 | 0.10 |
| Gym Users | 168.00 | 46.00 | 54.00 | 0.46 |
| Bowling Users | 102.00 | 46.00 | 54.00 | 0.38 |
| Users Cinema | 76.00 | 40.00 | 60.00 | 0.04 |
| Users Restaurants | 96.00 | 42.00 | 58.00 | 0.07 |
| General Mall consumer | 36.25 | 42.00 | 58.00 | 0.10 |

clothing stores, electronics stores, toy stores, book stores, and grocery stores. The shopping center features a floor area of 151'000 m² and a volume of 780'000 m³. Fig. 4 displays the scheme of the shopping mall. The main features of the mall are detected by means of several inspections. These inspections were aimed at assessing the features of the shopping mall, the types of shops, the electrical appliances installed, the HVAC systems installed, and the scheduling of the users. Given the size of the shopping mall, 41 clusters of users are considered. Each cluster includes shops with similar characteristics and is a thermal zone of the TRNSYS model. Each thermal zone may require heating and/or cooling energy. Therefore, at the same time, some zones may need heating energy and others cooling energy. Table 4 presents the features of the envelope of the selected shopping mall, assumed according to the above-mentioned inspections and to the constructive era of the shopping mall, i.e. 1989 [73]. To assess the user thermal load, both building space heating and cooling, the scheduling of the users of the shopping mall and the heat gains related to human activities inside the mall and to the electrical appliances installed are carefully modelled. Table 5 summarizes the main values related to the heat gains and to the average electrical consumption of the main devices installed in the different thermal zones of the shopping mall. The selection of these values is based on Refs. [74–76] and the inspections of the building. Note that the electrical appliances refer to the devices installed into each thermal zone, such as monitors, computers, small servers and so on. The lighting refers to the lights installed in each thermal zone.

Table 6 displays the main heat gains related to the consumers of the shopping mall. These heat gains differ among the shopping mall zones because a different behavior of the people in the defined zones is assumed [76,77].

Fig. 5 presents the weekly schedule of the users of the shopping mall. This figure presents the occupancy of the shopping mall. When the value is equal to 1, the maximum number of consumers is present in the shopping mall. The maximum number of consumers is assumed to be equal to 16'000 people. The shopping mall is open from 10 AM to 12 AM on working days, and from 11 AM to 9 PM on the weekend. These data were harvested by means of several inspections and from the feature of the Google Maps displaying the ratio of occupancy of a commercial facility [78]. This tool is adopted and considered reliable in assessing the occupancy of commercial facilities [79]. The heating period is from 1st October to 30th April. The setpoint temperature for the zones requesting

building space heating thermal energy is 20 ± 1 °C. The cooling period has no limitation according to [80,81] for commercial users. In particular, during the winter period (November–March) the zones requesting cooling energy are featured by a setpoint temperature of 22 ± 1 °C [80,81]. Conversely during the rest of the year, the zones requesting cooling energy have a setpoint of 26 ± 1 °C [80,81]. A rated fresh air flow rate of 2.6 m³/m²h is considered for the whole year for the entire building [16,32]. The considered facility consumes roughly 16.00 m³ of domestic hot water (DHW) per day [46].

The shopping mall is not equipped with suitable energy meters. Therefore, there is no available data regarding the time-dependent energy demands of electrical appliances, HVAC systems, lighting, etc. Similarly, time-dependent data about space heating and cooling demand are also not available, nor are any measurements about the activation of electrical appliances or the number of customers in the building. Neither the yearly energy bills are available, due to privacy issues. These data, however, are required to estimate the building space heating and cooling demand. Therefore, to carry out the simulations, a very well-established approach in literature was adopted. The time-dependent space heating and cooling demands are calculated using validated tools used for the simulation of buildings. In addition, the time-dependent data regarding the activation of electrical appliances and the turnout of the buildings are assessed based on the local regulation or literature data. The results obtained by the model are consistent with the measured data available in literature for similar users. The energy performance of the modelled user are calibrated against data available in open literature, for example Ref. [80].

The RS is based on a 1.50 MW internal combustion engine (Table 7), simultaneously producing thermal and electric energy. The thermal energy produced by the engine is used for providing thermal energy to the coils of the air handling units (AHUs) operating in heating mode. A natural gas fired boiler of 3.20 MW_{th} is included as auxiliary system. In addition, this thermal energy recovered from the engine is also used for producing cooling energy by means of a 0.96 MW_{th} absorption chiller. This cooling energy is delivered to the coils of the AHUs operating in cooling mode. A chiller of 6.20 MW_{th} is installed as auxiliary system, to provide cooling energy even when thermal energy produced by ACH is not sufficient. Finally, the thermal energy recovered from the engine is also used for producing domestic hot water (DHW). A natural gas boiler of 0.10 MW_{th} is installed as auxiliary system, Table 7.

The electricity produced by the cogenerator (CHP) partially matches the electricity demand of the shopping mall. Note that this plant also includes a small photovoltaic (PV) field of 0.21 MW, which matches a limited share of the yearly user electricity demand: i.e. 2% (Table 8). The selected user consumes almost 1.565×10^6 Sm³/y of natural gas and withdraws 7.23 GWh/y of electricity from the grid. In particular, the selected shopping mall consumes roughly 18.20 GWh/y of primary energy and has a yearly operating cost of 0.91 M€/y, Table 8.

The PS consists of the above-described shopping mall power plant, where the CHP is dismissed, and local heating/cooling network is modified to a 5th generation district heating and cooling (5GDHC) network. In particular, this plant includes two neutral rings (NR1 and

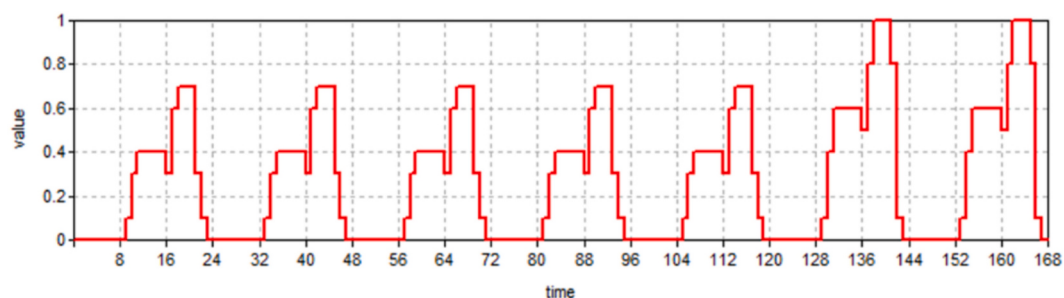


Fig. 5. Weekly schedule of the consumers of the shopping mall.

Table 7
Main components data of the plant.

| Component | Parameter | Description | Value | Unit |
|-------------------|-----------------|------------------------------------------------|----------------------------|-------------------|
| CB _H | $Q_{th,CBH}$ | Rated capacity of CB _H | 3.2 | MW _{th} |
| | $T_{set,CB}$ | Set point temperature for CB _H | 50 | °C |
| | η_{CBDHW} | CB _H efficiency | 86 | % |
| CB _{DHW} | $Q_{th,CBSHW}$ | Rated CB for SHW thermal flow rate | 0.10 | MW _{th} |
| | $T_{set,CBSHW}$ | Set point temperature for CB _{SHW} | 65 | °C |
| | η_{CBDHW} | CB _{SHW} efficiency | 0.86 | % |
| Cogenerator [82] | | Model Name | J-420-GS-B | |
| | | – | GE Jenbacher GmbH & Co OHG | |
| | Manufacturer | | | |
| ACH | $Q_{th,CHP}$ | Rated thermal capacity | 1.60 | MW |
| | $P_{el,CHP}$ | Rated electrical capacity | 1.50 | MW |
| | PE_{input} | Rated fuel input | 3.60 | |
| | η_{el} | Rated electrical efficiency | 41.70 | |
| | η_{th} | Rated thermal efficiency | 44.45 | % |
| CH | $Q_{th,rated}$ | Global rated efficiency | 86.16 | |
| | COP | Rated cooling capacity | 0.96 | MW _{th} |
| | COP | Rated coefficient of performance | 0.72 | – |
| CT (RS) | $Q_{th,CT}$ | Rated cooling capacity | 6.20 | kW |
| | N_{fans} | Number of fans | 4 | kW |
| | $P_{el,fans}$ | Rated fans electricity demand | 35 | |
| PV _{RS} | $P_{el,rated}$ | PV rated capacity for reference system | 0.21 | MW |
| | η_{PV} | Rated PV field efficiency | 18.00 | % |
| | $P_{el,rated}$ | PV rated capacity for proposed system | 5.40 | MW |
| PV _{PS} | η_{PV} | Rated PV field efficiency | 18.00 | % |
| | Cap_{LIB} | Lithium-ion battery rated capacity | 10.8 | MW |
| | V_{LIB} | Lithium-ion battery voltage | 360 | V |
| LIB | C_{cell} | Cell rated capacity | 63.27 | Ah |
| | SOC_{min} | Minimum allowed state of charge | 95.0 | % |
| | SOC_{max} | Maximum allowed state of charge | 5.0% | |
| M-HP1 | $Q_{th,rated}$ | Rated heating capacity | 6.30 | kW |
| | $P_{el,rated}$ | Rated power of heat pump in heating mode | 2.02 | kW |
| | COP | Rated COP | 3.09 | – |
| CTi (PS) | $m_{water,LS}$ | Rated water flow rate load side (condenser) | 1029 | m ³ /h |
| | $m_{air,SS}$ | Rated air flow rate source side (evaporator) | 693.33 | m ³ /s |
| | $P_{th,CT}$ | Rated cooling tower capacity | 3.90 | MW |
| WLHP H | N_{fans} | Number of fans | 2 | – |
| | $P_{el,fans}$ | Rated fans electricity demand | 60 | kW |
| | $NCTs$ | Number of identical cooling towers | 3 | – |
| WLHP C | $Q_{th,rated}$ | Rated heating capacity | 1.25 | MW |
| | $P_{el,rated}$ | Rated power of heat pump in heating mode | 0.27 | MW |
| | COP | Rated COP | 4.63 | – |
| WLHP C | $m_{water,LS}$ | Rated water flow rate load side (condenser) | 217.84 | m ³ /h |
| | $m_{water,SS}$ | Rated water flow rate source side (evaporator) | 288.37 | m ³ /h |
| | N_{HPS} | Number of heat pumps operating in heating mode | 4 | |
| WLHP C | $Q_{th,rated}$ | Rated heating capacity | 1.14 | MW |
| | $P_{el,rated}$ | Rated power of heat pump in heating mode | 0.22 | MW |
| | COP | Rated COP | 5.11 | – |
| WLHP C | $m_{water,LS}$ | Rated water flow rate load side (evaporator) | 196.52 | m ³ /h |
| | $m_{water,SS}$ | Rated water flow rate source side (condenser) | 233.81 | m ³ /h |
| | N_{HPS} | Number of heat pumps operating in cooling mode | 6 | |

Table 7 (continued)

| Component | Parameter | Description | Value | Unit |
|-----------|----------------|----------------------------------------------|--------|-------------------|
| HP DHW | $Q_{th,rated}$ | Rated heating capacity | 115.70 | kW |
| | $P_{el,rated}$ | Rated power of heat pump in heating mode | 36.40 | kW |
| | COP | Rated COP | 3.18 | – |
| | $m_{water,LS}$ | Rated water flow rate load side (condenser) | 20.00 | m ³ /h |
| | $m_{air,SS}$ | Rated air flow rate source side (evaporator) | 10.23 | m ³ /s |

NR2 in Fig. 2). As mentioned above, NR1 represents the cold sink for the heat pumps (HPs) operating in heating mode. In particular, this ring is balanced by a 6.20 MW_{th} air-to-water HP. NR1 feeds a group of four 1.25 MW_{th} water-to-water heat pumps (WWHPs) operating in heating mode, Table 7.

NR2 represents the hot sink for the heat pumps (HPs) operating in cooling mode. This ring is balanced by means of three 3.80 MW_{th} cooling towers. The neutral ring 2 (NR2) withdraws thermal energy from the condensers of six water-to-water heat pumps of 1.15 MW_{th} operating in cooling mode, Table 7. Neutral ring 1 (NR1) is designed for operating within the temperature range 15.5 °C - 19.0 °C, while NR2 operates within the design range 18.5 °C - 24.0 °C.

Since the domestic hot water demand for a shopping mall is extremely limited, a small, dedicated 4th generation district heating (4GDH) loop is considered. This loop is based on an air-to-water heat pump (AWHP) of 115.5 kW_{th}.

As the energy demand of the proposed system is entirely matched by electricity, the photovoltaic (PV) field capacity was increased from 0.20 MW in the reference system to 5.40 MW in the proposed system. Moreover, a lithium-ion battery of 10.80 MWh is installed to increase the shopping mall self-sufficiency, Table 7.

5. Results

Table 8 presents the annual performance of the proposed system, highlighting a significant decrease in grid dependence. This is primarily due to the small amount of electricity withdrawn from the grid ($E_{el,fromGRID}$), equal to 0.97 GWh/y (Table 8). In particular, the electricity self-consumed ($E_{el,self}$) by the system matches almost 87% of the total electricity demand (Table 8), which encompasses both the load of the shopping mall and the electricity demand due to HVAC systems. Consequently, the combination of the PV field and the battery storage system substantially reduces the grid electricity usage. Fig. 6 further highlights these findings, showing that on both typical winter and summer days, the majority of the mall energy needs are met through self-produced electricity ($P_{el,self}$).

On a typical summer day, the PV power production ($P_{el,PV}$) significantly exceeds the plant energy consumption ($P_{el,LOAD}$). As a result, the lithium-ion battery is charged ($P_{el,toLIB}$) from 7 AM to 5 PM with a peak power of 2.70 MW. From 5 PM, the battery ($P_{el,fromLIB}$) discharges to meet the load of the shopping mall. Note that $P_{el,LOAD}$ sharply increases at 9 AM, coinciding with the shopping mall opening, as discussed in the Case Study section. Therefore, there is no need to withdraw electricity from the grid on a typical summer day.

Conversely, on a typical winter day, due to the lower solar availability, the electricity withdrawn from the grid ($P_{el,fromGRID}$) matches $P_{el,LOAD}$ only in the late evening because the system cannot fully charge the battery during daylight.

Fig. 7 and Fig. 8 show the monthly electric energy performance of the proposed system and Fig. 9 shows the monthly variations of the thermal energy demand. The trends above discussed are confirmed in Fig. 7 and Fig. 8, where the electricity withdrawn from the grid ($E_{el,fromGRID}$) remains below 0.13 GWh/month. In particular, except for January and December (Fig. 8), $E_{el,fromGRID}$ matches less than 17% of the shopping

Table 8
Yearly performance of the reference and proposed systems.

| Parameter | Description | Reference System | Proposed System | Unit |
|-------------------------------|------------------------------------------------------------------------------------|-----------------------|-----------------|---------------------|
| | | Value | | |
| $E_{el,baseLOAD}$ | District electricity demand | 4.57 | 4.57 | GWh/y |
| $E_{el,LOAD}$ | Overall system electricity load | 7.23 | 7.64 | GWh/y |
| $E_{el,fromGRID}$ | Electricity withdrawn from the grid | 1.53 | 0.97 | GWh/y |
| $E_{el,toGRID}$ | Electricity exported to the grid | 0.03 | 0.97 | GWh/y |
| $E_{el,self}$ | Electricity self-consumed | 5.70 | 6.67 | GWh/y |
| $E_{el,CHP}$ | Electricity produced by the CHP | 5.56 | — | GWh/y |
| $E_{th,CHP,useful}$ | Useful thermal energy produced by CHP | 5.50 | — | GWh/y |
| $E_{el,PV}$ | Electricity produced by PV field | 0.14 | 8.80 | GWh/y |
| $E_{el,fromLIB}$ | Electricity withdrawn from the lithium-ion battery (LIB) | — | 2.28 | GWh/y |
| $E_{el,toLIB}$ | Electricity exported to the LIB | — | 2.87 | GWh/y |
| $E_{el,M-HP1}$ | Electricity consumption of the heat pump M-HP1 | — | 0.11 | GWh/y |
| $E_{th,M-HP1}$ | Thermal energy produced by the heat pump M-HP1 | — | 0.42 | GWh/y |
| $E_{el,CTs}$ | Electricity demand of the cooling tower (CT) | — | 0.64 | GWh/y |
| $E_{th,CTs}$ | Thermal energy rejected by the CT | — | 8.95 | GWh/y |
| $E_{el,RO}$ | Electricity demand of the reverse osmosis (RO) unit | — | 0.05 | GWh/y |
| M_{DW} | Demineralized water consumed by the CT | — | 11,865.24 | m ³ /y |
| $E_{el,WLHP-H}$ | Electricity consumption of water loop heat pump operating in heating mode (WLHP-H) | — | 0.22 | GWh/y |
| $E_{th,WLHP-H}$ | Thermal energy produced by WLHP-H | — | 1.10 | GWh/y |
| $E_{el,WLHP-C}$ | Electricity consumption of water loop heat pump operating in cooling mode (WLHP-C) | — | 1.30 | GWh/y |
| $E_{th,WLHP-C}$ | Thermal energy produced by WLHP-C | — | 7.78 | GWh/y |
| $E_{th,M-HE}$ | Thermal energy transferred by the main heat exchanger (M-HE) | — | 0.46 | GWh/y |
| $E_{th,H,demand}$ | Thermal energy demand for heating | 1.09 | 1.09 | GWh/y |
| $E_{th,C,demand}$ | Thermal energy demand for cooling | 7.76 | 7.76 | GWh/y |
| PE | Primary Energy consumption | 18.06 | 0.00 | GWh/y |
| $V_{NG,CHP}$ | Natural gas consumed by the CHP | 1.468 10 ⁶ | — | Sm ³ /y |
| V_{NG} | Volume of natural gas consumed | 1.565 10 ⁶ | — | Sm ³ /y |
| C | Operating costs | 0.91 | 0.14 | M€/y |
| ΔC | Operating costs difference | — | 0.61 | M€/y |
| C_{inv} | Capital costs | — | 11.18 | M€ |
| SPB | Simple Payback | — | 14.19 | y |
| NPV | Net Present Value | — | 0.56 | M€ |
| PI | Profit Index | — | 0.05 | — |
| CO_2 | CO ₂ emissions | 3840 | 659 | tCO ₂ /y |
| $E_{el,fromGRID}/E_{el,LOAD}$ | Electric energy ratio: electricity from grid on system load | — | 12.69 | % |
| $E_{el,fromLIB}/E_{el,LOAD}$ | Electric energy ratio: electricity from LIB on system load | — | 29.90 | % |

Table 8 (continued)

| Parameter | Description | Reference System | Proposed System | Unit |
|----------------------------|-----------------------------------------------------------------------------------------------|------------------|-----------------|------|
| | | Value | | |
| $E_{el,self}/E_{el,LOAD}$ | Electric energy ratio: self-consumed electricity on system load | — | 87.31 | % |
| $E_{el,toLIB}/E_{el,PV}$ | Electric energy ratio: electricity delivered to LIB on the electricity production | — | 32.62 | % |
| $E_{el,toGRID}/E_{el,PV}$ | Electric energy ratio: electricity delivered to grid on the electricity production | — | 11.02 | % |
| $E_{el,self}/E_{el,PV}$ | Electric energy ratio: self-consumed electricity on the electricity production | — | 75.74 | % |
| COP_{M-HP1} | Coefficient of performance M-HP1 | — | 3.86 | — |
| COP_{WLHP-H} | Coefficient of performance WLHP-H | — | 4.93 | — |
| COP_{WLHP-C} | Coefficient of performance WLHP-C | — | 5.97 | — |
| $E_{el,RO}/E_{el,CTS,tot}$ | Electric energy ratio: electricity consumed by RO unit on the electricity consumed by the CTs | — | 6.89 | % |
| $E_{th,M-HE}/E_{th,toNR1}$ | Thermal energy ratio: thermal energy exchanged in M-HE on the thermal energy demand of NR1 | — | 51.12 | % |
| $E_{th,M-HE}/E_{th,toNR2}$ | Thermal energy ratio: thermal energy exchanged in M-HE on the thermal energy demand of NR2 | — | 1.47 | % |
| $PES_{H\&C}$ | Primary Energy Saving only considering heating and cooling energy demand | — | 11.19 | % |
| PES | Primary Energy Saving | — | 100.02 | % |
| R_{new} | Ratio of renewable fraction | — | 89.23 | % |
| ΔC | Operating costs difference | — | 82.83 | % |
| ΔCO_2 | CO ₂ emissions savings | — | 100.01 | % |

mall monthly energy needs ($E_{el,LOAD}$). In fact, in January and December, $E_{el,fromGRID}$ meets 23% and 42% of the shopping mall energy demand ($E_{el,LOAD}$), respectively. This result is related to the integration of the 5GDHC network, which converts thermal demand into electric load. During these months, i.e. January and December, the thermal energy demand for heating is maximum (Fig. 9) but at the same time the PV electricity production is at its lowest (Fig. 7 and Fig. 8).

However, the peak in thermal energy demand occurs in the summer period, when the cooling energy demand achieves its maximum value of 1.48–1.64 GWh/month, Fig. 9. During the summer months the photovoltaic power production also peaks, Fig. 7, allowing the proposed system to fully leverage the increase in renewable electricity production. In fact, during the summer period the electricity self-consumed ($E_{el,self}$) achieves the maximum value of 0.79–0.83 GWh/month, matching averagely 86% of the system electricity load on monthly basis (Fig. 8).

For these reasons, the electricity exported to the grid is extremely limited, i.e. 0.97 GWh/y. In fact, the plant self-consumes the majority of the renewable electricity produced, exploiting the high capacity of the battery. Especially during July and August, the months of peak photovoltaic production, the plant utilizes nearly all of the PV-generated electricity, resulting in almost zero export to the grid during these periods, Fig. 8.

The months with the highest share of surplus electricity are March, April, and May, due to the reduced HVAC systems demands, i.e. space cooling and space heating demand limited (Fig. 9), and the PV production is increasing, Fig. 7 and Fig. 8. As a result, during these months, both primary energy consumption (PE) and operating costs (C_{op}) for the mall are negative. In fact, the electricity withdrawn from the grid is significantly lower than the electricity exported to the grid, as shown by

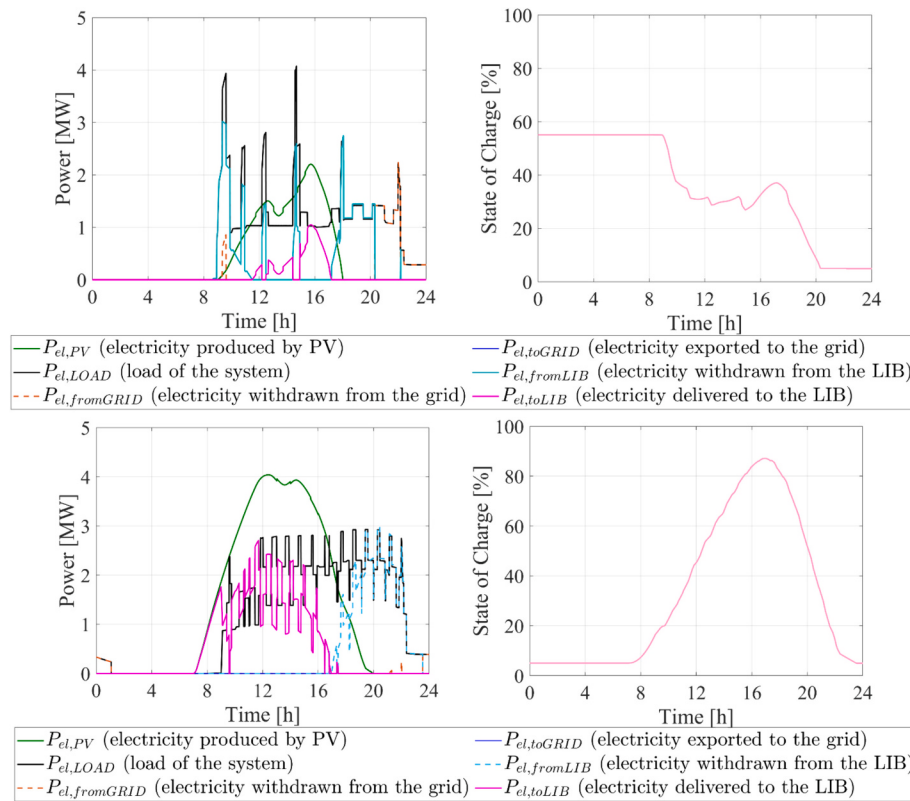


Fig. 6. Power results for a typical winter day (above) and a typical summer day (below).

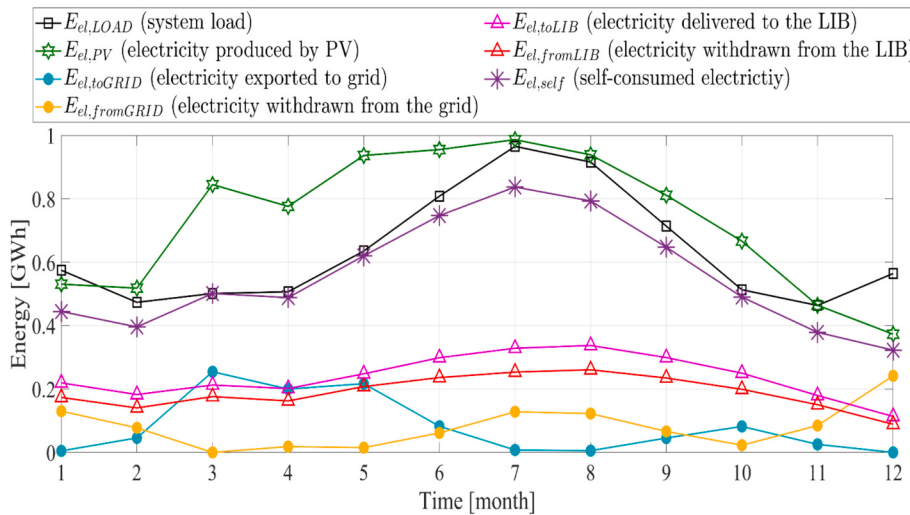


Fig. 7. Monthly electric energy performance of the proposed system: electricity fluxes.

Fig. 10 which displays the primary energy and operating costs on a monthly basis.

The remarkable profitability achieved by this plant is also due to the use of the 5GDHC network. In fact, the thermal energy exchanged between first neutral ring (NR1) and the second neutral ring (NR2) through the main heat exchanger, $E_{th,M-HE}$, (M-HE in Fig. 2), accounts for approximately 51% of the thermal energy required to balance NR1 ($E_{th,NR1}$). In particular, Fig. 11 shows the dynamic operation of the main heat exchanger. During the operation of the water loop heat pumps operating in heating mode, WLHPs-H, (see Fig. 2 and System Layout section), the heat exchange is allowed according to the control strategy described in detail in section System Model (Fig. 3). Thanks to this, the temperature of

the water exiting the WLHPs-H evaporators ($T_{NR1,inM-HE}$) increases by roughly 4.0 °C in the early morning. In particular, NR2 discharges about 1.10–2.15 MW_{th} to NR1 (Q_{M-HE} in Fig. 11), being able to balance NR1 without activating the main heat pump M-HP1 (see also Fig. 2). However, from 11 AM to 11:26 AM the M-HP1 is activated to balance NR1, with a peak of heat transfer rate (Q_{M-HE1}) of 6.02 MW_{th}. This is due to the insufficient thermal energy provided by NR2 for balancing NR1, Fig. 11.

Regarding neutral ring 2 (NR2), the heat exchange enables this ring to operate with a temperature ranging from 14.0 °C to 17.0 °C, Fig. 11. This temperature range is significantly lower than the rated range, i.e. 18.5 °C – 24.0 °C (see System Layout section). However, the actual temperature range (14.0 °C – 17.0 °C) is consistent with the water loop

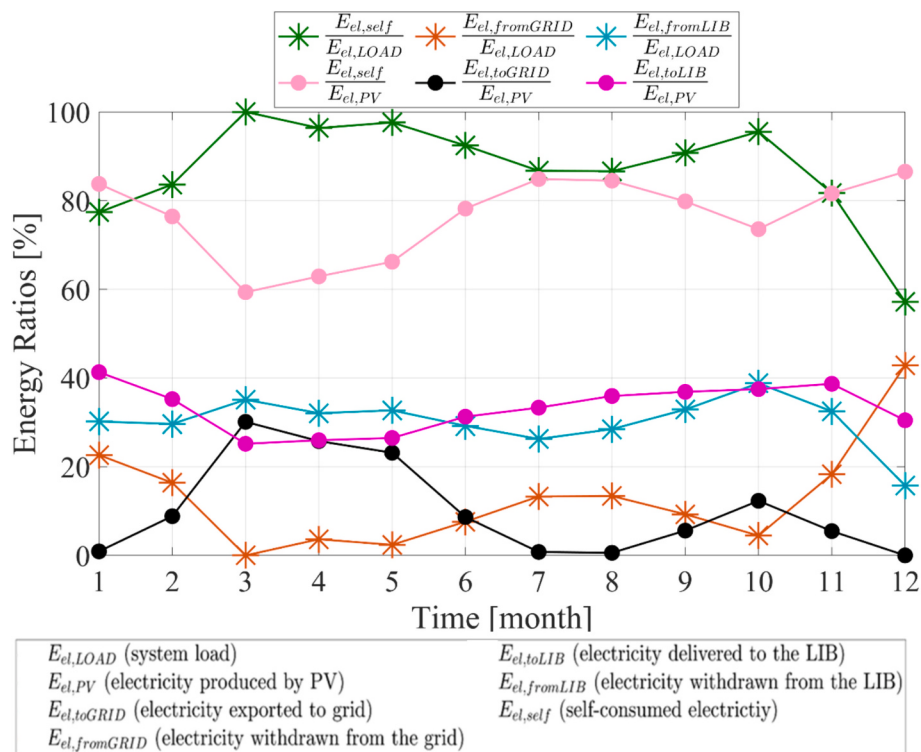


Fig. 8. Monthly electric energy performance of the proposed system: electric energy ratio.

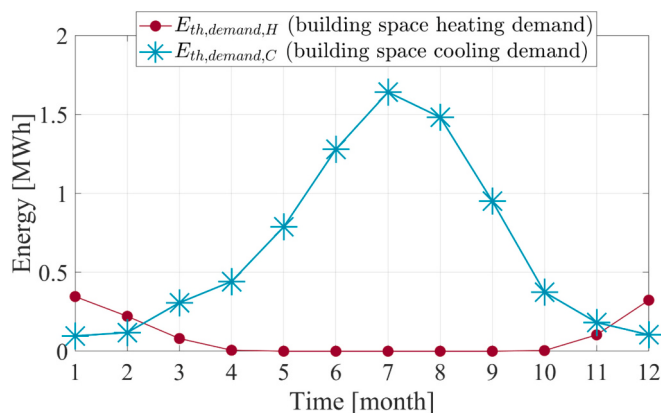


Fig. 9. Monthly thermal energy demand of the analyzed user.

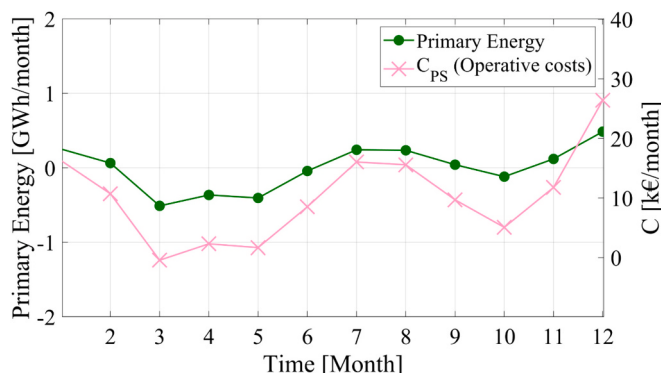


Fig. 10. Primary energy and operating costs on a monthly basis.

heat pumps operating in cooling mode (WLHPs-C) condenser operating temperatures, i.e., 10.0 °C – 45.0 °C. Being the temperature of NR2 remarkably lower than the rated one, WLHPs-C can operate with extremely favorable conditions. As a result, the WLHPs-C achieves a COP of 7.00 during the coldest months (from December to February). Fig. 12 shows the COPs of the heat pumps operating in the substations. The monthly COP of the water loop heat pumps operating in heating mode (WLHPs-H) is quite constant and equal to 5.00, Fig. 12. This trend results from the control strategy adopted, which allows the WLHPs-H evaporators to work with a nearly constant operating temperature.

The COP of the water loop heat pumps operating in cooling mode (WLHPs-C) decreases as the space heating demand decreases. This trend is consistent with the previous observations where the heat exchange occurring in the M-HE significantly reduces the temperature of neutral ring 2 (NR2) below its rated range. As space heating demand decreases, the thermal energy discharged by NR2 to NR1 decreases. Therefore, the temperature of NR2 increases, lowering the COP of the WLHPs-C.

During the summer period, the cooling towers (CTs) hardly keep the neutral ring 2 temperature (T_{NR2}) within the rated range, due to the higher ambient temperature and humidity, causing NR2 temperature to exceed the upper bound of its operating range, i.e. 24.0 °C. This results in a reduction of the COP of the water loop heat pumps operating in cooling mode (WLHPs-C) to relatively low values: 5.53 and 5.60 in July and August, respectively (Fig. 12). Therefore, the cooling towers prove to be suited for balancing NR2. In fact, these can balance NR2 consuming less electricity than an air-to-water heat pumps (AWHPs) group. Their use only leads to a limited reduction of the summer performance of the cooling network, since the temperature of NR2 rises above the upper limit of the rated temperature operating range. However, the increase in water loop heat pumps electricity consumption, due to the lower COP, is overcome by the fact that the electricity supplied to the CTs fans is lower, when compared with the electricity that would have to be supplied to an air-to-water HP.

The demineralized water consumption, i.e. reverse osmosis unit (RO), only marginally affects the energy performance of the whole system. In fact, the electricity delivered to the reverse osmosis unit for

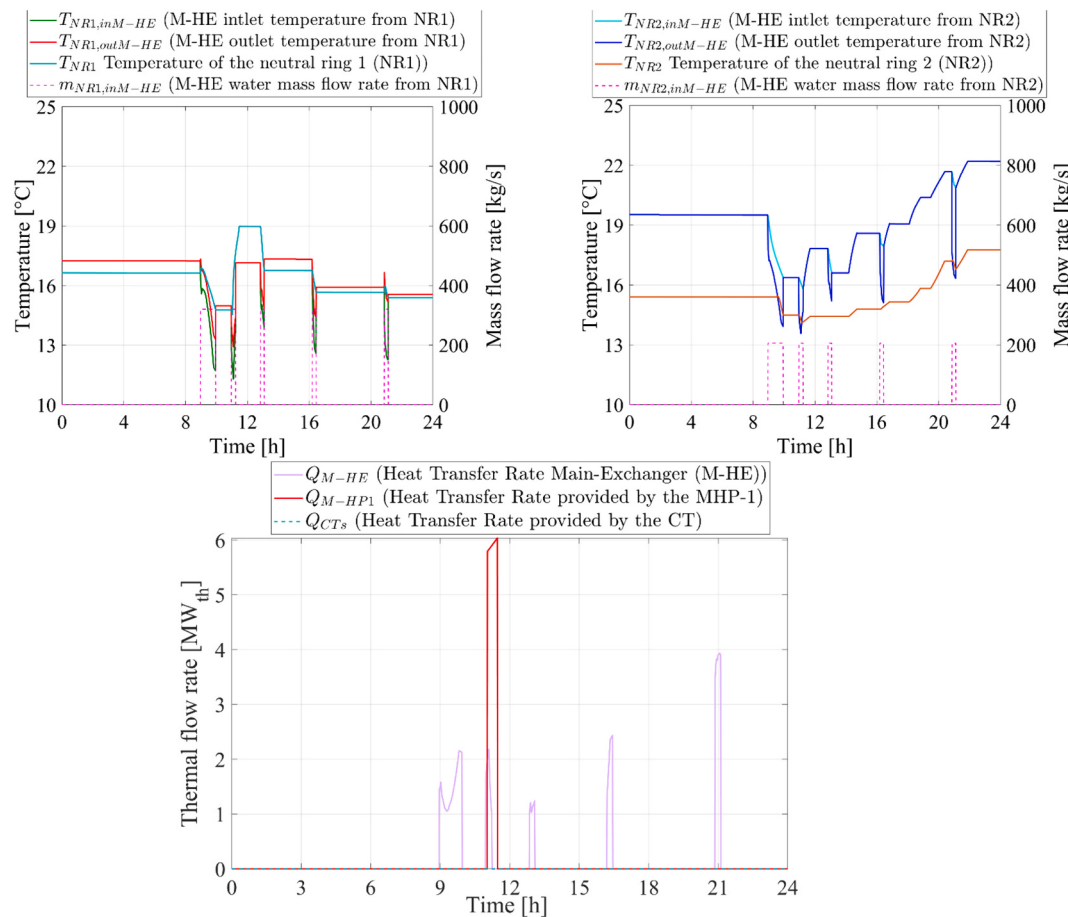


Fig. 11. Dynamic results during a typical winter day: heat transfer rate performance of the main heat exchanger (M-HE) (above), and contribution of main heat pump (M-HP1) and cooling tower (CT) to the thermal energy performance of neutral ring 1 (NR1), (below).

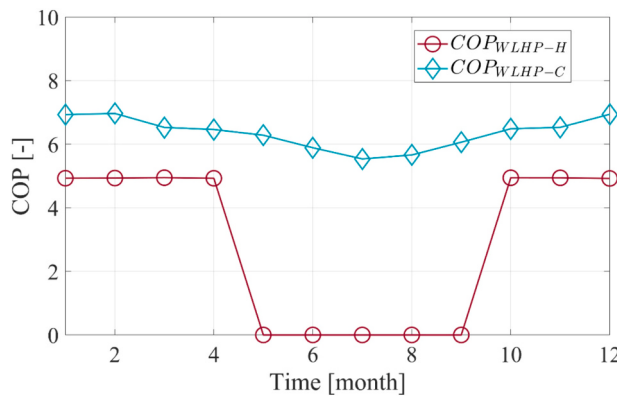


Fig. 12. COPs of the heat pumps operating in the substations: COP of the water loop heat pumps operating in heating mode (COP_{WLHP-H}) and COP of the water loop heat pumps operating in cooling mode (COP_{WLHP-C}).

the production of demineralized water ($E_{el,RO}$) only accounts for roughly 6.5% of the electricity supplied to the cooling towers ($E_{el,CTs,tot}$, Table 8). Fig. 13 and Fig. 14 show the monthly thermal energy performance of the 5th generation district heating network. On a yearly basis, the thermal energy provided by the M-HE supplies a negligible contribution to the thermal energy required for driving neutral ring 2 (NR2), with $E_{th,M-HE}/E_{th,NR2}$ equal to nearly 1% (Table 8). This result is primarily due to the fact that this heat exchange only occurs when a simultaneous demand for space heating and space cooling energy exists. However, from

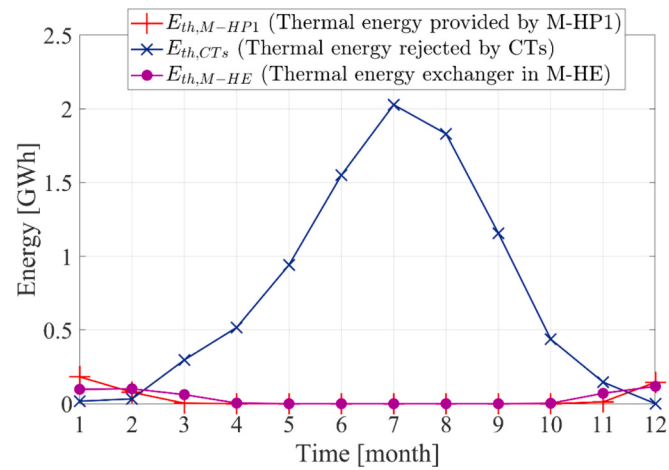


Fig. 13. Monthly thermal energy performance of the 5th generation district heating network: energy fluxes.

November to February, the $E_{th,M-HE}$ matches more than 80% of the NR2 thermal energy demand (Fig. 14). Conversely, in the summertime only the cooling towers (CTs) balance NR2, Fig. 14. Another reason for this result is due to the thermal energy demand of NR2 is significantly greater than NR1. In fact, NR2 achieves a peak of thermal energy demand of 2.00 GWh_{th}/month in summer ($E_{th,CTS}$ Fig. 13), whereas NR1 achieves a peak of thermal energy demand of 0.18 GWh_{th}/month during winter ($E_{th,M-HP1}$ Fig. 13). Therefore, the thermal energy recovered by

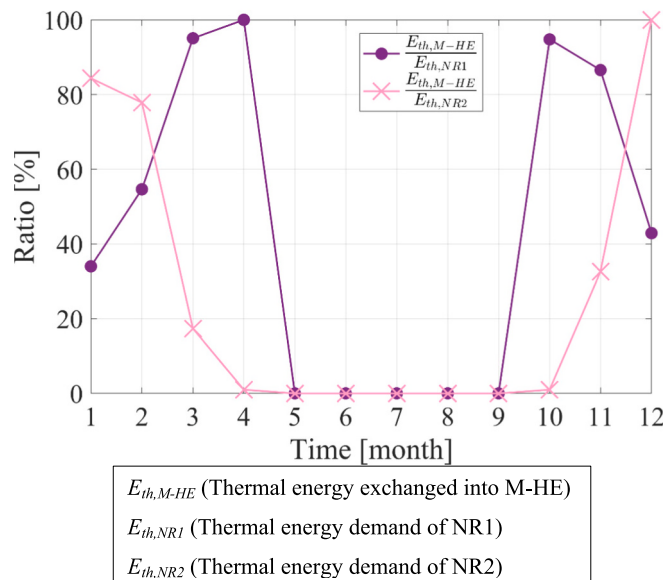


Fig. 14. Monthly thermal energy performance of the 5th generation district heating network: energy ratio.

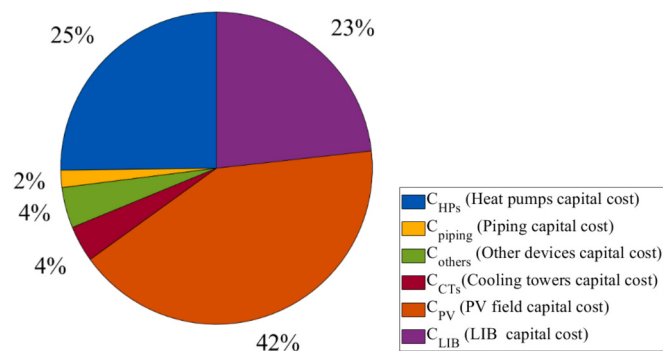


Fig. 15. Cost figures of the proposed plant.

means of M-HE, i.e., 0.46 GWh_{th}/y, is much lower than the thermal energy demand of NR2, i.e., $E_{th,CTs}$ is equal to 8.95 GWh_{th}/y, Table 8.

In conclusion, the proposed system reaches very interesting energy results with a primary energy saving (*PES*) of 100%, Table 8. This result is related with the equation used for evaluating the primary energy saving index, see Eq.(2a). However, without considering the surplus electricity, the renewable energy matches roughly 89% of the shopping mall demand, see R_{new} Table 8 (Eq.(2b)).

From an economic point of view, the proposed system achieves

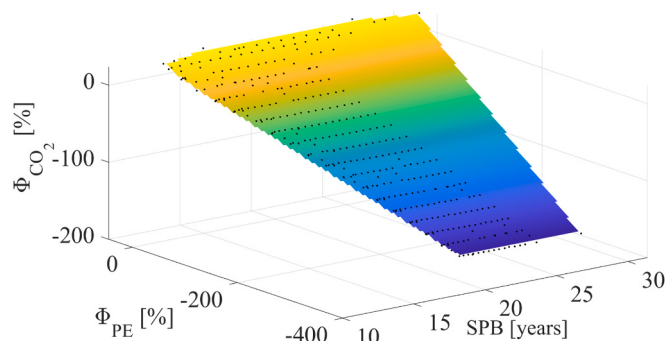


Fig. 16. Optimal configuration research and Pareto frontier: objective functions: primary energy (Φ_{PE}), Simple Payback (SPB), and CO_2 emissions (Φ_{CO_2}).

average results, with a Simple Payback (*SPB*) of 15.2 years (Table 8). This result is because, in Spain, intensive energy users can sign energy purchasing contracts featured by relatively low prices. In fact, in this framework, the electricity purchasing cost is equal to 0.09 €/kWh and the natural gas purchasing cost is equal to 0.53 €/Sm³. Therefore, the mall has relatively low operating costs. The proposed system reduces the operating costs of the mall by 82.83%, because the self-consumed energy matches roughly 87% of the mall energy demand. However, this reduction is shadowed by the remarkable high capital cost of the plant, i.e., 11.2 M€ (Table 8). The heat pumps (HPs) account for 25% of the overall capital cost (C_{inv}) of the plant, while the PV field weights for 42% of the C_{inv} (Fig. 15). The fact that the piping network accounts for a limited share of the capital cost relies on the fact that the mall has a relatively limited extension, and then a limited piping network is needed. It is worth of nothing that, very different results would be achieved in Italy, where much higher energy prices are detected; here the *SPB* would be roughly 5 years.

Sensitivity analysis.

A sensitivity analysis is performed to study the effect of thermal energy storage installed in neutral ring 1 (NR1) and neutral ring 2 (NR2). The capacity of the tank varies from 50 m³ to 750 m³. The analysis showed that the effect of the thermal energy storage is quite negligible on the overall system performance. In fact, the detected variation of Simple Payback (*SPB*) and Primary Energy Saving (*PES*) was lower than 0.5%. This is due to the fact that the system operates with a very narrow operative range of temperatures.

In order to assess which is the best layout, a sensitivity analysis is carried out. In particular, the capacity of the photovoltaic (PV) field varies from 2.70 MW to 21.60 MW, while the capacity of the battery is changed from 5.40 MWh to 43.20 MWh.

Fig. 16 shows the Pareto frontier considering the objective functions: primary energy (Φ_{PE}), CO_2 emissions (Φ_{CO_2}), and Simple Payback (*SPB*), see System model. As expected, this figure highlights that the lower the Φ_{PE} , the lower Φ_{CO_2} is. At the same time the layouts featuring the lower Φ_{PE} and Φ_{PE} achieve extremely poor economic results. Note that according to the equations used for defining Φ_{PE} and Φ_{CO_2} (Eq.(5a) and Eq. (5b)) these objective functions can be negative when the primary energy demand and the equivalent CO_2 emissions of the proposed system are negative. This may occur when the renewable energy produced by the system is greater than the fossil based imported energy, see also Eq.(2a) and Eq.(2d). Therefore, the lowest values of Φ_{PE} and Φ_{CO_2} are achieved in a system characterized by a very high capacity of PV field and battery. This configuration results in a minimal amount of electricity being withdrawn from the grid and a significantly high amount of excess electricity being delivered to the grid. However, due to the extremely low prices for purchasing and exporting electricity, such system is not economically profitable. The high capital costs of high-capacity systems are not offset by the savings achieved.

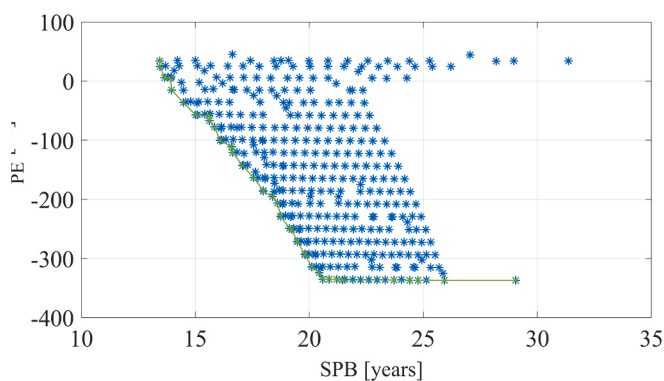


Fig. 17. Optimal configuration research and Pareto frontier: objective functions: primary energy (Φ_{PE}) and Simple Payback (SPB).

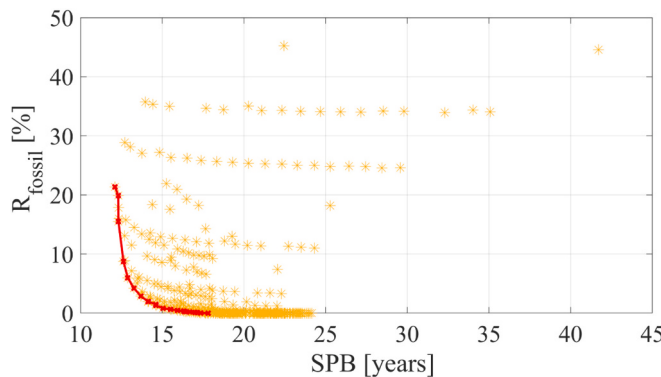


Fig. 18. Optimal configuration research and Pareto frontier: objective functions: percentage of the mall load met by nonrenewable energy (R_{fossil}) and Simple Payback (SPB).

To better understand this trend, in Fig. 17 the Pareto frontier only for the Simple Payback (SPB) and the primary energy (ϕ_{PE}) objective functions is displayed. Fig. 17 confirms that configurations with the minimum ϕ_{PE} yield poor economic outcomes. However, the optimal configuration identified on the Pareto frontier features a ϕ_{PE} of 5.80% and a SPB of 13.65 years. This optimal layout includes a PV capacity of 4.32 MW and a battery capacity of 4.40 MWh, with the system primary energy consumption being 5.80% of the reference system. Therefore, the system can be considered almost self-sufficient. Note that increasing the battery capacity and/or the photovoltaic (PV) field capacity would decrease ϕ_{PE} , reducing the system primary energy consumption and significantly increasing the excess electricity delivered to the grid ($E_{el,towGRID}$). However, the higher investment costs associated with larger PV and battery capacities are not balanced by the increased savings, due to the low price of exported electricity.

To further analyze and connect the sensitivity analysis with self-consumed energy, the Pareto Frontier is presented, focusing on Simple Payback (SPB) and R_{fossil} as objective functions, in Fig. 18. R_{fossil} , defined in Eq.(2b), excludes surplus electricity, and closely correlates with self-consumed energy. For instance, an R_{fossil} of 0%, indicates that the system load is entirely met by renewable energy. In this context, Fig. 18 confirms that the most effective layout includes a photovoltaic (PV) field of 4.32 MW and a battery of 4.40 MWh, achieving a R_{fossil} of 21.36% and a Simple Payback (SPB) of 13.45 years. This means that in this optimal configuration, only 21% of the user primary energy demand is matched by non-renewable sources. Further increases in PV and battery capacity result in more self-consumed energy. However, this improvement is marginal, offering a limited reduction in operating costs. Consequently, further reductions in R_{fossil} , i.e. a higher capacity system, worsen the economic performance. These trends confirm that increasing the capacity of the renewable plant reduces the economic performance, due to the low prices for electricity purchasing and exporting. Finally, for the

sake of clarity, Fig. 19 displays the trends of R_{renew} and SPB, by mutually varying battery capacity and PV field capacity. These results are consistent with the discussions above carried out. Again, the higher the capacity of the renewable power plant, the higher the SPB. Notably, for a PV field capacity above 6.47 MW and a battery capacity over 13.00 MWh, more than 97% of the mall load is matched by renewable energy, rendering the system almost energy independent.

Carbon Taxes.

Finally, the effect of carbon tax policies is investigated. The carbon tax is an economic penalty related to the equivalent CO₂ emissions of the user. In particular, the carbon tax specific value (j_{CO2}) is changed from 0 €/kgCO_{2,eq} to 10 €/kgCO_{2,eq}. Given that for the PS the electricity withdrawn from the grid ($E_{el,fromGRID}$ Table 8), and delivered to the grid ($E_{el,toGRID}$ Table 8), are almost equal to 0.97 GWh/y, the overall equivalent CO₂ emissions of the proposed system (PS) are almost equal to zero. For this reason, the carbon tax does not affect the operating costs of the PS (C_{PS}), Fig. 20. Conversely, such a policy significantly reduces the economic performance of the reference system RS (C_{RS}), Fig. 20. In particular, when j_{CO2} is greater than 2 €/kgCO_{2,eq}, the additional cost due to carbon tax accounts for more than 55% of the overall operating costs of the existing plant, Fig. 20. Therefore, as j_{CO2} rises, the simple payback (SPB) dramatically decreases. For j_{CO2} greater than 1.00 €/kgCO_{2,eq} the SPB is lower than 7.90 years, making the proposed system profitable from an economic point of view, Fig. 21.

In conclusion, proper carbon tax policies are a suitable tool for pushing energy-intensive users to adopt energy measures that significantly reduce their primary energy consumption and environmental impact.

6. Conclusions

This paper proposes a novel layout of a 5th generation district heating cooling network, based on two neutral rings. The first ring provides thermal energy to the evaporators of the heat pumps operating in heating mode. The second ring withdraws thermal energy from the condenser of the heat pumps operating in cooling mode. The heat exchange between the two rings is allowed by means of the main heat exchanger. This heat exchange is the core of the 5th generation technology, allowing the condensers of the heat pumps operating in cooling mode to transfer heat to the evaporators of the heat pumps operating in heating mode. This 5th generation district heating and cooling network is integrated with a photovoltaic field and a lithium-ion battery. These are designed with the aim of meeting the power load of the selected user, which also includes the electricity demand for driving the 5th generation district heating cooling network.

The end user is a large shopping mall located in Madrid. The thermal energy demands of the several zones of the shopping mall are matched by means of air handling units. The features of the end user are carefully assessed and modelled by means of several inspections. The performances of the end user are calibrated against open literature data.

The dynamic simulation model is developed in TRNSYS 18

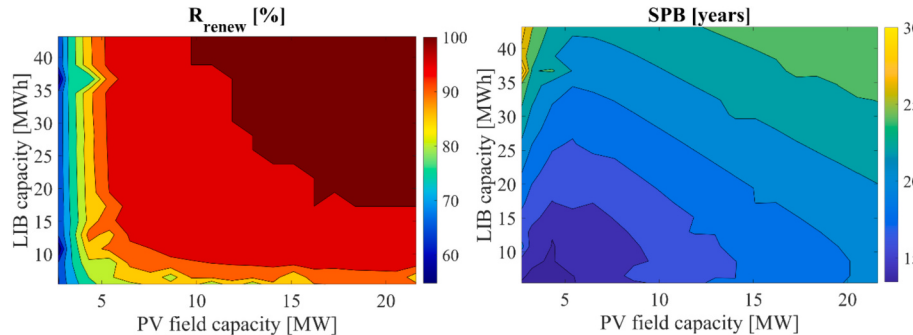


Fig. 19. Sensitivity analysis: percentage of the mall load matched by renewable energy (R_{renew}) and Simple Payback (SPB).

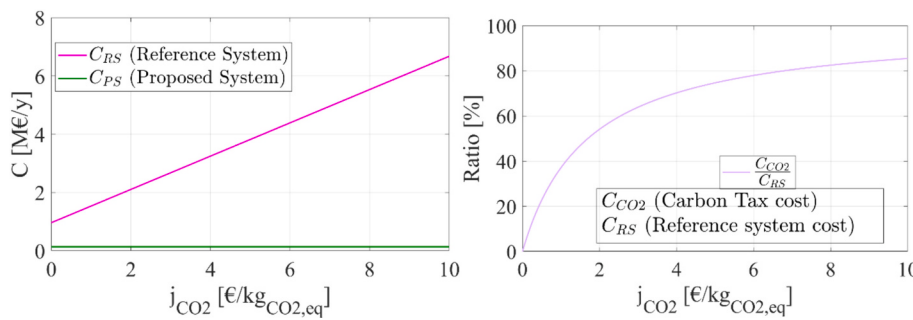


Fig. 20. Carbon tax results: operating costs (C) and carbon tax cost (C_{CO2}).

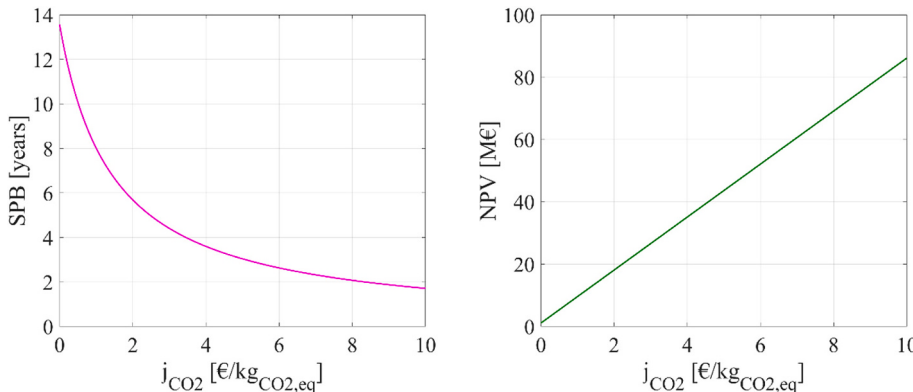


Fig. 21. Carbon tax results: operating costs.

environment. The main results achieved in this work are listed below.

- The proposed system has a great energy and environmental impact since it has the potential to reduce the primary energy consumption of the user by 89%.
- In Spain large energy users can sign very convenient energy purchasing contracts. In this framework, the selected user is favored by very low energy purchasing prices. For this reason, the proposed system features average economic results with a simple payback period of 14.19 years.
- The cooling towers are suited for balancing the warm neutral ring of the 5th generation district heating and cooling network. In fact, cooling towers can steer the ring temperature within the rated range for most of the time, with a very limited electricity consumption. Only during the hottest summer days, the ring temperature rises above the upper bound of the rated range. This only leads to a limited worsening of the chillers performance. In fact, the COP of the heat pump operating in cooling mode changes from the maximum value of 6.9 (January–February) to the minimum value of 5.5 (July–August).
- The novel 5th generation layout proposed in this research maximizes the thermal energy exchange from the condenser of the heat pumps operating in cooling mode and the evaporator of the heat pumps operating in heating mode. In fact, the thermal energy recovered by means of the main heat exchanger provides 51% of the thermal energy needed for driving the ring one, i.e. the cold sink of the heat pumps operating in heating mode.
- The optimal response surface analysis highlights that, due to the low energy purchasing prices, the capacity of the photovoltaic field and the battery should be limited to 4.32 MW and 2.40 MWh, respectively. Larger photovoltaic field and battery capacity result in the worsening of the economic performance. The increase in capital cost is not balanced by the reduction in operating costs.

- Carbon tax policies confirms to be a suitable tool for pushing the adoption of renewable based energy measure able to significantly reduce the primary energy consumption of large end users. In fact, for a carbon tax greater than 1.00 €/kg CO_2,eq the simple payback period is lower than 7.9 years.

In conclusion, 5th generation district heating and cooling network suits facilities featured by a significant contemporaneity between heating and cooling load. Therefore, this technology may be considered a profitable measure to reduce the environmental impact and the operating costs of shopping malls. In this framework carbon tax policy should be considered for pushing forward the adoption of renewable based and high efficiency energy measures.

CRediT authorship contribution statement

Francesco Calise: Writing – review & editing, Validation, Supervision, Software, Resources, Project administration, Methodology, Funding acquisition, Formal analysis, Conceptualization. **Francesco Liberato Cappiello:** Writing – review & editing, Writing – original draft, Visualization, Validation, Supervision, Software, Resources, Project administration, Methodology, Investigation, Funding acquisition, Formal analysis, Data curation, Conceptualization. **Luca Cimmino:** Writing – review & editing, Writing – original draft, Visualization, Software, Investigation, Data curation. **Maria Vicidomini:** Writing – review & editing, Validation, Resources, Methodology, Investigation, Data curation. **Fontina Petrakopoulou:** Writing – review & editing, Visualization, Validation, Supervision, Resources, Investigation, Data curation.

Declaration of competing interest

The corresponding author confirms that all the other authors have read and approved the manuscript and no ethical issues and conflict of

interest are involved. In particular the authors confirm that have no known competing financial interests or personal relationships that could have appeared to influence the work reported in this paper.

Data availability

Data will be made available on request.

Acknowledgements

The authors gratefully acknowledge the partial financial support of the project "Sustainable Energy Networks" CUP E65F21003190003.

The authors gratefully acknowledge the partial financial support of the project PRIN 2020: OPTIMISM – Optimal refurbishment design and management of small energy micro-grids, funded by the Italian Ministry of University and Research (MUR).

References

- [1] Golmohamadi H, Larsen KG. Economic heat control of mixing loop for residential buildings supplied by low-temperature district heating. *J Building Engin* 2022;46: 103286.
- [2] Jodeiri AM, Goldsworthy MJ, Buffa S, Cozzini M. Role of sustainable heat sources in transition towards fourth generation district heating – A review. *Renew Sust Energ Rev* 2022;158:112156.
- [3] Wang Y, Zhang S, Chow D, Kuckelkorn JM. Evaluation and optimization of district energy network performance: present and future. *Renew Sust Energ Rev* 2021;139: 110577.
- [4] Büning F, Wetter M, Fuchs M, Müller D. Bidirectional low temperature district energy systems with agent-based control: performance comparison and operation optimization. *Appl Energy* 2018;209:502–15.
- [5] Piacentino A, Catrini P, Cardona F. Chapter 3 - methodologies for the evaluation of polygeneration systems. In: Calise F, Dentice D'Accadia M, Vanoli L, Vicidomini M, editors. Polygeneration Systems. Academic Press; 2022. p. 79–115.
- [6] Reiners T, Gross M, Altieri L, Wagner H-J, Bertsch V. Heat pump efficiency in fifth generation ultra-low temperature district heating networks using a wastewater heat source. *Energy* 2021;236:121318.
- [7] Puttige AR, Andersson S, Östin R, Olofsson T. Modeling and optimization of hybrid ground source heat pump with district heating and cooling. *Energ Build* 2022;264: 112065.
- [8] Wu D, Jiang J, Hu B, Wang RZ. Experimental investigation on the performance of a very high temperature heat pump with water refrigerant. *Energy* 2020;190: 116427.
- [9] von Rhein J, Henze GP, Long N, Fu Y. Development of a topology analysis tool for fifth-generation district heating and cooling networks. *Energy Convers Manag* 2019;196:705–16.
- [10] Gjoka K, Rismanchi B, Crawford RH. Fifth-generation district heating and cooling systems: A review of recent advancements and implementation barriers. *Renew Sust Energ Rev* 2023;171:112997.
- [11] Sulzer M, Werner S, Mennel S, Wetter M. Vocabulary for the fourth generation of district heating and cooling. *Smart Energy* 2021;1:100003.
- [12] Gong Y, Ma G, Jiang Y, Wang L. Research progress on the fifth-generation district heating system based on heat pump technology. *Journal of Building Engineering* 2023;71:106533.
- [13] Buffa S, Cozzini M, D'Antoni M, Baratieri M, Fedrizzi R. 5th generation district heating and cooling systems: A review of existing cases in Europe. *Renew Sust Energ Rev* 2019;104:504–22.
- [14] Lund H, Østergaard PA, Nielsen TB, Werner S, Thorsen JE, Gudmundsson O, et al. Perspectives on fourth and fifth generation district heating. *Energy* 2021;227: 120520.
- [15] Østergaard DS, Smith KM, Tunzi M, Svendsen S. Low-temperature operation of heating systems to enable 4th generation district heating: A review. *Energy* 2022; 248:123529.
- [16] Lund H, Østergaard PA, Chang M, Werner S, Svendsen S, Sorknæs P, et al. The status of 4th generation district heating: research and results. *Energy* 2018;164: 147–59.
- [17] Zhang Y, Johansson P, Sasic Kalagasidis A. Assessment of district heating and cooling systems transition with respect to future changes in demand profiles and renewable energy supplies. *Energy Convers Manag* 2022;268:116038.
- [18] Barco-Burgos J, Bruno JC, Eicker U, Saldaña-Robles AL, Alcántar-Camarena V. Review on the integration of high-temperature heat pumps in district heating and cooling networks. *Energy* 2022;239:122378.
- [19] Abokersh MH, Saikia K, Cabeza LF, Boer D, Vallès M. Flexible heat pump integration to improve sustainable transition toward 4th generation district heating. *Energy Convers Manag* 2020;225:113379.
- [20] Mi P, Zhang J, Han Y, Guo X. Study on energy efficiency and economic performance of district heating system of energy saving reconstruction with photovoltaic thermal heat pump. *Energy Convers Manag* 2021;247:114677.
- [21] Ji Q, He H, Kennedy S, Wang J, Peng Z, Xu Z, et al. Design and evaluation of a wind turbine-driven heat pump system for domestic heating in Scotland. *Sustain Energy Technol Assess* 2022;52:101987.
- [22] Aliana A, Chang M, Østergaard PA, Victoria M, Andersen AN. Performance assessment of using various solar radiation data in modelling large-scale solar thermal systems integrated in district heating networks. *Renew Energy* 2022;190: 699–712.
- [23] Sun F, Hao B, Fu L, Wu H, Xie Y, Wu H. New medium-low temperature hydrothermal geothermal district heating system based on distributed electric compression heat pumps and a centralized absorption heat transformer. *Energy* 2021;232:120974.
- [24] Romanov D, Leiss B. Geothermal energy at different depths for district heating and cooling of existing and future building stock. *Renew Sust Energ Rev* 2022;167: 112727.
- [25] Soltero VM, Quirosa G, Peralta ME, Chacartegui R, Torres M. A biomass universal district heating model for sustainability evaluation for geographical areas with early experience. *Energy* 2022;242:122954.
- [26] Pieper H, Kirs T, Krupenski I, Ledvanov A, Lepiksaar K, Volkova A. Efficient use of heat from CHP distributed by district heating system in district cooling networks. *Energy Rep* 2021;7:47–54.
- [27] Sun F, Li J, Fu L, Li Y, Wang R, Zhang S. New configurations of district heating and cooling system based on absorption and compression chillers driven by waste heat of flue gas from coke ovens. *Energy* 2020;193:116707.
- [28] Jebamalai JM, Marlein K, Laverge J. Design and cost comparison of district heating and cooling (DHC) network configurations using ring topology – A case study. *Energy* 2022;258:124777.
- [29] Abugabbara M, Javed S, Bagge H, Johansson D. Bibliographic analysis of the recent advancements in modeling and co-simulating the fifth-generation district heating and cooling systems. *Energ Build* 2020;224:110260.
- [30] Brown A, Foley A, Laverty D, McLoone S, Keatley P. Heating and cooling networks: A comprehensive review of modelling approaches to map future directions. *Energy* 2022;261:125060.
- [31] Wirtz M, Heleno M, Moreira A, Schreiber T, Müller D. 5th generation district heating and cooling network planning: A Dantzig-Wolfe decomposition approach. *Energy Convers Manag* 2023;276:116593.
- [32] Falay B, Schweiger G, O'Donovan K, Leusbroek I. Enabling large-scale dynamic simulations and reducing model complexity of district heating and cooling systems by aggregation. *Energy* 2020;209:118410.
- [33] Hirsch H, Nicolai A. An efficient numerical solution method for detailed modelling of large 5th generation district heating and cooling networks. *Energy* 2022;255: 124485.
- [34] Sorknæs P, Østergaard PA, Thellufsen JZ, Lund H, Nielsen S, Djørup S, et al. The benefits of 4th generation district heating in a 100% renewable energy system. *Energy* 2020;213:119030.
- [35] Pipiciello M, Trentin F, Soppelsa A, Menegon D, Fedrizzi R, Ricci M, et al. The bidirectional substation for district heating users: experimental performance assessment with operational profiles of prosumer loads and distributed generation. *Energ Build* 2024;113872.
- [36] Li X, Yilmaz S, Patel MK, Chambers J. Techno-economic analysis of fifth-generation district heating and cooling combined with seasonal borehole thermal energy storage. *Energy* 2023;285:129382.
- [37] Bu T, Fan R, Zheng B, Sun K, Zhou Y. Design and operation investigation for the fifth-generation heating and cooling system based on load forecasting in business districts. *Energ Build* 2023;294:113243.
- [38] Bellos E, Iliadis P, Papalexis C, Rotas R, Nikolopoulos N, Kosmatopoulos E, et al. Dynamic investigation of centralized and decentralized storage systems for a district heating network. *Journal of Energy Storage* 2022;56:106072.
- [39] Dorotić H, Puškec T, Duić N. Multi-objective optimization of district heating and cooling systems for a one-year time horizon. *Energy* 2019;169:319–28.
- [40] Bordignon S, Quaggiotto D, Vivian J, Emmi G, De Carli M, Zarrella A. A solar-assisted low-temperature district heating and cooling network coupled with a ground-source heat pump. *Energy Convers Manag* 2022;267:115838.
- [41] Akkurt GG, Aste N, Borderon J, Buda A, Calzolari M, Chung D, et al. Dynamic thermal and hygrometric simulation of historical buildings: critical factors and possible solutions. *Renew Sust Energ Rev* 2020;118:109509.
- [42] Carotenuto A, Figari RD, Vanoli L. A novel solar-geothermal district heating, cooling and domestic hot water system: dynamic simulation and energy-economic analysis. *Energy* 2017;141:2652–69.
- [43] Edtmayer H, Nageler P, Heimrath R, Mach T, Hohenauer C. Investigation on sector coupling potentials of a 5th generation district heating and cooling network. *Energy* 2021;230:120836.
- [44] Fiorentini M, Heer P, Baldini L. Design optimization of a district heating and cooling system with a borehole seasonal thermal energy storage. *Energy* 2023;262: 125464.
- [45] MacCarrini A, Sotnikov A, Sommer T, Wetter M, Sulzer M, Afshari A. Influence of building heat distribution temperatures on the energy performance and sizing of 5th generation district heating and cooling networks. *Energy* 2023;275:127457.
- [46] Testasecca T, Catrini P, Beccali M, Piacentino A. Dynamic simulation of a 4th generation district heating network with the presence of prosumers. *Energy Conversion and Management*: X 2023;20:100480.
- [47] Saini P, Huang P, Fiedler A, Volkova X, Zhang.. Techno-economic analysis of a 5th generation district heating system using thermo-hydraulic model: A multi-objective analysis for a case study in heating dominated climate. *Energ Build* 2023; 296:113347.
- [48] Calise F, Cappiello FL, Dentice d'Accadia M, Pettrakopoulou F, Vicidomini M. A solar-driven 5th generation district heating and cooling network with ground-

- source heat pumps: a thermo-economic analysis. *Sustain Cities Soc* 2022;76:103438.
- [49] Calise F, Cappiello FL, Cimmino L, Dentice d'Accadia M, Vicidomini M. Renewable smart energy network: A thermoeconomic comparison between conventional lithium-ion batteries and reversible solid oxide fuel cells. *Renew Energy* 2023;214:74–95.
- [50] Cappiello FL, Erhart TG. Modular cogeneration for hospitals: A novel control strategy and optimal design. *Energy Convers Manag* 2021;237:114131.
- [51] Klein S, Beckman W, Mitchell J, Duffie J, Duffie N, Freeman TJATSSPUOW. Madison. Solar energy laboratory, TRNSYS. 2006.
- [52] Abdel-Dayem AM, Hawawi YM. Feasibility study using TRANSYS modelling of integrating solar heated feed water to a cogeneration steam power plant. *Case Studies in Thermal Engin* 2022;39:102396.
- [53] Bordignon S, Emmi G, Zarrella A, De Carli M. Energy analysis of different configurations for a reversible ground source heat pump using a new flexible TRNSYS type. *Appl Therm Eng* 2021;197:117413.
- [54] Gölt O, Çam NY, Alptekin E, Ezan MA, Erek A. Development of an integrated underfloor heating system model in TRNSYS and performance assessments. *Journal of Energy Storage* 2024;84:110993.
- [55] Rana A, Gröf G. Assessment of prosumer-based energy system for rural areas by using TRNSYS software. *Cleaner Energy Sys* 2024;8:100110.
- [56] Żoładek M, Figaj R, Sornek K. Energy analysis of a micro-scale biomass cogeneration system. *Energy Convers Manag* 2021;236:114079.
- [57] Sui X, Liu H, Du Z, Yu S. Developing a TRNSYS model for radiant cooling floor with a pipe-embedded PCM layer and parametric study on system thermal performance. *Journal of Energy Stor* 2023;71:108024.
- [58] Murray MC, Finlayson N, Kummert M, Macbeth J. Live energy TRNSYS–TRNSYS simulation within google SketchUp. 2009.
- [59] Calise F, Cappiello FL, Dentice d'Accadia M, Vicidomini M. Dynamic simulation, energy and economic comparison between BIPV and BIPVT collectors coupled with micro-wind turbines. *Energy* 2020;191:116439.
- [60] Arshad N, Alhajaj A. Process synthesis for amine-based CO₂ capture from combined cycle gas turbine power plant. *Energy* 2023;274:127391.
- [61] Mucci S, Mitsos A, Bongartz D. Power-to-X processes based on PEM water electrolyzers: A review of process integration and flexible operation. *Comput Chem Eng* 2023;175:108260.
- [62] Calise F, Cappiello FL, Dentice d'Accadia M, Vicidomini M. Smart grid energy district based on the integration of electric vehicles and combined heat and power generation. *Energy Convers Manag* 2021;234:113932.
- [63] Ahmed S, Trask SE, Dees DW, Nelson PA, Lu W, Dunlop AR, et al. Cost of automotive lithium-ion batteries operating at high upper cutoff voltages. *J Power Sources* 2018;403:56–65.
- [64] Selectrica. Tarifa TUR gas. <https://tarifasgasluz.com/comparador/tarifa-ultimo-recurso-gas>; 2023.
- [65] A.D.E.C.G.C.D. ENERGÍA. Barometro Energetico. <https://www.aege.es/barometro-energetico-espana/>; 2023.
- [66] E.E. Agency. Greenhouse gas emission intensity of electricity generation in Europe. <https://www.eea.europa.eu/en/analysis/indicators/greenhouse-gas-emission-in-tensity-of-1>; 2023.
- [67] Calise F, Cappiello FL, Dentice d'Accadia M, Vicidomini M. Thermo-economic optimization of a novel hybrid renewable trigeneration plant. *Renew Energy* 2021;175:532–49.
- [68] Fisher RA, Fisher RA, Genetiker S, Fisher RA, Genetician S, Britain G, et al. The design of experiments. Oliver and Boyd Edinburgh. 1966.
- [69] Friso A, Galvanin F. An optimization-free Fisher information driven approach for online design of experiments. *Comput Chem Eng* 2024;187:108724.
- [70] Wetter M. GenOpt—A Generic Optimization Program. Seventh international IBPSA conference. 2001. pp. 601–8.
- [71] Agrawal A, Pandey SN, Srivastava L. Pareto-frontier differential evolution based financial approach for multi-objective congestion management using customer participation and on-site generation. *Renewable Energy Focu* 2022;42:253–65.
- [72] Ahmadi P, Dincer I. 1.28 energy optimization. In: Dincer I, editor. Comprehensive energy systems. Oxford: Elsevier; 2018. p. 1085–143.
- [73] Zhang M, Liu J, Zhang Y-H, Wang L, Li J-L, Hong J-P. Preparation of highly dispersed silicon spheres supported cobalt-based catalysts and their catalytic performance for Fischer-Tropsch synthesis. *J Fuel Chem Technol* 2023;51:608–15.
- [74] Ballal V, Cavalett O, Cherubini F, Watanabe MDB. Climate change impacts of e-fuels for aviation in Europe under present-day conditions and future policy scenarios. *Fuel* 2023;338:127316.
- [75] Rackley SA. 5 - carbon capture from industrial processes. In: Rackley SA, editor. Carbon capture and storage (second edition). Boston: Butterworth-Heinemann; 2017. p. 103–14.
- [76] R. American Society of Heating, E. Air-Conditioning. ASHRAE handbook : fundamentals. GA: ASHRAE, Atlanta; 1993. p. 1993.
- [77] Nemmour A, Inayat A, Janajreh I, Ghani C. Green hydrogen-based E-fuels (E-methane, E-methanol, E-ammonia) to support clean energy transition: A literature review. *Int J Hydrog Energy* 2023;48(75).
- [78] Google. Popular times, wait times, and visit duration. <https://support.google.com/business/>; 2020.
- [79] Nejadshamsi S, Eicker U, Wang C, Bentahar J. Data sources and approaches for building occupancy profiles at the urban scale – A review. *Build Environ* 2023;238:110375.
- [80] M.C.T. Tolmasquim, A.S. Szkoł, J.B.J.E.c. Soares, management.. Economic potential of natural gas fired cogeneration plants at malls in Rio de Janeiro 2001; 42:663–74.
- [81] Espana GD. Real Decreto 1027/2007 -, <https://www.boe.es/buscar/act.php?id=BOE-A-2007-15820>. in: M.d.I. Presidencia, (Ed.).29/02/2008.
- [82] Jenbacher-Werke. Innio - CHP, <https://www.innio.com/en/products/jenbacher>. 2019.